Double-Polyelectrolyte, Like-Charged Amphiphilic Diblock Copolymers: Swollen Structures and pH- and Salt-Dependent Lyotropic Behavior

Denis D. Bendejacq*,† and Virginie Ponsinet‡

Rhodia Aubervilliers Research and Technological Centre, Consumer Care Laboratory, 52 Rue de la Haie Coq, 93308 Aubervilliers, France, and Université Bordeaux 1, CNRS, Centre de Recherche Paul Pascal UPR 8641, Avenue Schweitzer, 33600 Pessac, France

Received: December 21, 2007; Revised Manuscript Received: March 13, 2008

We consider a symmetrical poly(styrene-*stat*-(acrylic acid))-*block*-poly(acrylic acid), i.e., PSAA-*b*-PAA, diblock copolymer, with a molar fraction $\varphi_{AA} = 0.42$ of acrylic acid, in the more hydrophobic PSAA statistical first block. We investigate its structural behavior at constant concentration in water using small-angle neutron scattering (SANS) by varying (i) the ionization of its acrylic acid motives via the pH by adding NaOH and (ii) the ionic strength of the solution by increasing the NaCl salt concentration c_S. We present the resulting morphological phase diagram {pH, c_S}, in which we identified two different lamellar phases presenting a smectic long-range order at small-to-intermediate ionizations and a spherical phase with a liquidlike short-range order at larger ionization. In the low-ionization regime, the first lamellar phase comprises a water-free PSAA lamellar core surrounded by a dense poly(acrylic acid) brush swollen with water. Its mostly hydrophobic core still being glassy, this phase is unable to reorganize and is frozen in. A detailed analysis of the SANS data shows the osmotic nature of the polyelectrolyte brush, in which the Na^+ counterions are confined so that local electroneutrality is satisfied. Above the pH at which the PSAA statistical block starts ionizing, the PSAA lamellar core melts. The second lamellar phase identified then comprises a PSAA core thinner than that of the frozen-in previous phase, implying a significant increase of the core/water interface and a decrease of the brush surface density. The transition from the first lamellar phase to the second one can be quantitatively shown to result from the balance between the two contributions: (i) the extra interfacial cost between the thinner core and water and (ii) the associated gain in entropy of mixing for the counterions confined inside the brush. At even higher ionization, the diblocks finally form spherical objects with a very small, pH-dependent aggregation number and reach an apparent onset of self-association. When the highest ionization investigated is reached, the cores of these final spherical core−shell objects are found to contain a significant amount of water. We thereby demonstrate that at constant concentration, pH, and ionic strength both trigger a transition from frozen to molten hydrophobic phases as well as unexpected morphological transitions.

1. Introduction

Very much like small-molecule surfactants, amphiphilic block copolymers placed in a selective solvent comprise solvophobic and solvophilic antinomical moieties, and it was found early on that they could form self-assembled structures. Let us recall that the most fundamental properties of small-molecule surfactants are their dynamic behavior, the existence of self-assembled structures as well as their interfacial activity.[1] For a large enough concentration in water called the critical micellar concentration (cmc), surfactants reach thermodynamic equilibrium via a continuous exchange between self-assembled structures, referred to as "micelles", and a non-negligible population of free (nonassociated) amphiphiles. The self-assembly process derives from the minimization of the enthalpic cost of contacting the solvent molecules and the solvophobic tails, at the expense of the entropy of mixing of the surfactants. For even higher concentrations, surfactant molecules also often display ordered phases, direct or inverse, such as cubic, hexagonal, or smectic phases. The latter are referred to as lyotropic, for their symmetry mostly depends on concentration, although other solution conditions such as temperature, ionic strength, or pH may have an effect.

The concepts of an enthalpically driven self-assembly, of a cmc and of a truly dynamic behavior, were readily adopted for block copolymers, then called polymeric surfactants (or macrosurfactants).[2] The most well-known and documented example is that of the poly(ethylene oxide)-*block*-poly(propylene oxide) (PEO/PPO) block copolymers.[3] Yet, very few other block copolymers have been found to actually display the fundamental properties of surfactants. Although it is appealing, the diblock/surfactant analogy overlooks the true polymeric nature of the two moieties and the dramatic impact that large molecular weights could have on their behavior. The cmcs (commonly reported at extremely small values[4]), as well as a truly dynamic behavior, are even suspected to be nonexistent for amphiphilic block copolymers,[5] which form structures unable to reversibly reorganize by themselves when submitted to conventional triggers (pH, ionic strength, concentration) that truly surfactant structures would usually react to. As a result, the structures formed are often referred to as "frozen-in". These features have somewhat restricted applicative developments for amphiphilic block copolymers. Most importantly, they have greatly limited the scope of the experimental investigations and the understand-

* To whom correspondence should be addressed. E-mail: denis.bendejacq@eu.rhodia.com.
† Rhodia Aubervilliers Research and Technological Centre.
‡ Université Bordeaux 1.

10.1021/jp712015h CCC: $40.75
Published on Web 06/17/2008

ing of their solution behavior until it was shown that morphological transitions could be studied provided "keys" were found to unlock the frozen frustrated state.[6] In spite of these practical drawbacks, these out-of-equilibrium, diblock copolymer structures still attract a lot of attention, for instance in the fields of latex synthesis,[7] stabilization,[8] rheology,[9] and drug delivery.[10,11] The high flexibility in copolymer design and the different synthetic routes now available, especially those based on controlled radical polymerization techniques like MADIX,[12–14] offer unmatched possibilities. Environmental constraints as well as bio-oriented material developments have promoted synthesis, formulation, and use of water-dispersible polymers, among which charged diblock copolymers are one of the most promising candidates. In particular, the possibility of playing on the morphological phase diagram, and therefore the rheological, conductivity, etc., properties via external stimuli such as pH or ionic strength, have long been looked after and have been recently well documented at a theoretical level.[15] Sensibility to pH or ionic strength requires charged polymeric segments, which adds another fundamental difference between polymeric and small-molecule amphiphiles.

Indeed, with diblocks comprising a polyelectrolyte block, the condition of local electroneutrality inside the coronal brush imposes an extensive confinement of the counterions. As a result, the brush chains are fully stretched and ensure maximum entropy of mixing for the confined counterions, as verified in many experimental cases.[16] This genuine feature of polyion assemblies has led to theoretical descriptions[17–19] dedicated to the physics of these particular objects called polyelectrolyte brushes, with no equivalence in the field of surfactant (mono)ion assemblies.

An extensive confinement has another important consequence: the large osmotic pressure associated with a confined counterion cloud is a strong drive to further increase, if allowed, the curvature of the core/corona interface and, thus, the counterion entropy of mixing inside the brush.[6,20] It is then no surprise that, in the literature, most charged diblock copolymer structures are generally spherical in symmetry, while their surfactant counterpart would display phases of all symmetries in similar conditions. Only very few studies have indeed been reporting on the existence of anisotropic phases in charged amphiphilic block copolymers and even less on the existence of such phases with long-range order, to the best of our knowledge. No complete experimental mapping of a phase diagram presenting pH- or salt-dependent lyotropic behaviors has ever been published, in contrast with well-documented effects of concentration in neutral diblock copolymers in selective solvents.[21] Tendencies were clearly evidenced with morphologies of dilute solutions quenched in water from a neutral solvent.[22,23] Spherical-to-cylindrical and spherical-to-lamellar transitions were visualized in dilute solutions of poly(acrylic acid)-block-poly(butadiene) (PAA-*b*-PBD), allowing the mapping of a morphological phase diagram[24] when pH and salt were varied. However, in the latter case, concentration was kept low in order to visualize isolated objects, and no long-range ordered anisotropic phase could be present.

In our previous investigations, we mapped out the dispersion behavior of amphiphilic glassy-polyelectrolyte poly(styrene)-*block*-poly(acrylic acid) (PS-*b*-PAA) diblock copolymers of different symmetries in water. The latter form out-of-equilibrium, frozen-in colloidlike objects unable to reorganize by themselves in water when pH or salt are varied, even though their coronas showed highly pH- and salt-sensitive responses. Later on, we also showed that modifying the composition of the hydrophobic block by copolymerizing styrene with acrylic acid motives could alter the frozen nature of the self-assembly. Indeed, once a large enough fraction of AA is introduced in the hydrophobic glassy PS block, an asymmetrical poly(styrene-*stat*-acrylic acid)-*block*-poly(acrylic acid) (PSAA-*b*-PAA) diblock showed features associated with a surfactant-like behavior: core−corona micelles were found at a large enough concentration, while their signature in small-angle neutron scattering (SANS) was observed to disappear upon dilution under a critical concentration on the order of 1−2 wt %, suggesting the existence of a cmc. However, due to the asymmetry of the diblock used, which comprised a large PAA block as the majority component, we were bound to find only core−corona objects of spherical symmetry, leaving the existence of anisotropic objects and ordered phases to a hope. We now combine the two principles, in a chemically tuned, symmetrical PSAA-*b*-PAA diblock copolymer. In the present article, we report on the mapping of the lyotropic phase diagram in water of this amphiphilic double-polyelectrolyte, like-charged diblock, varying pH and ionic strength at constant concentration. We first present SANS experiments allowing the partial mapping of a complex pH- and salt-dependent phase diagram. The latter displays two ordered anisotropic phases as well as the more classical spherical one. We then discuss the origin and physics of the structural transitions from one phase to another and consider a mean-field model, which takes into account each of the three contributions relevant for the system free energy: the stretching of the core blocks, the repulsive interactions between the corona-forming blocks and the interfacial energy between the core and the corona.

2. Experimental Section

Synthesis and Characterization. Previous papers[25,26] have detailed the emulsion synthesis via the MADIX technique proprietary of Rhodia,[12–14] of the poly(styrene-*stat*-ethylacrylate)-block-poly(ethylacrylate) diblock copolymer and its statistical precursor poly(styrene-*stat*-ethylacrylate) first block used in the present study. Their hydrolysis and purification provide the PSAA and PSAA-*b*-PAA copolymers of the present study. The latter are characterized by the following features: (i) a molar fraction $\varphi_{AA} = 0.42$ of acrylic acid in the PSAA first block; (ii) PSAA and PAA blocks of similar molecular weights, i.e., 8.3 and 9.5 kg/mol, with polydispersity indices of approximately 2.0. The weight fraction of the first PSAA block in the diblock is $w_{PSAA} = 0.465$, while the corresponding volume fraction is $f_{PSAA} = 0.549$. The diblock is thus nearly symmetrical. Finally, the diblock is denoted $(S_{53}A_{39})$-*b*-A_{133}, where 53, 39, and 133 are the average numbers of styrene and acrylic acid motives of the first block and that of acrylic acid motives of the second block, respectively. On the other hand, a homopolymer of acrylic acid denoted A_{111} is used as a reference for the second block of the diblock. It was synthesized separately, using the MADIX technology in solution in ethanol, and has a molecular weight of 8.0 kg/mol and index of molecular polydispersity of 1.4.

Solid films of $(S_{53}A_{39})$-*b*-A_{133} were cast from tetrahydrofuran (THF) solutions at concentration 15−20 wt %, in poly(tetrafluoroethylene) molds. They were placed overnight under vacuum at room temperature and heated for an hour at 60 °C to remove traces of THF. The final films were 0.2−0.4 mm thick. Small-angle X-ray scattering (SAXS) and transmission electron microscopy (TEM) experiments carried out on the films[26] demonstrated that $(S_{53}A_{39})$-*b*-A_{133} forms a lamellar phase (L) in the melt state, comprising stacked $(S_{53}A_{39})$ and A_{133} bilayers. The melt period d_M of this smectic phase, half-

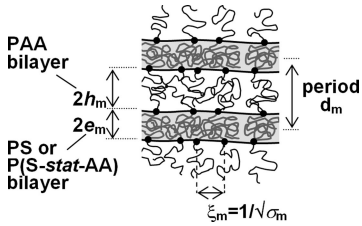

Figure 1. Schematic illustration of lamellar (L) phases formed in the melt state by symmetrical diblock copolymers $(S_{53}A_{39})$-*b*-A_{133} and S_{83}-*b*-A_{123}.

thicknesses e_M and h_M of, respectively, the $(S_{53}A_{39})$ and A_{133} bilayers, and finally the melt surface area per chain ξ_M^2 (inverse of the brush density σ_M) are represented in Figure 1 and their values summarized in Table 1.

Finally, we introduce the symmetrical diblock copolymer S_{83}-*b*-A_{123}, whose behavior has been detailed in a previous study.[27] This copolymer has approximately the same total molecular weight, but it comprises a pure poly(styrene) first block (cf. Table 1 for characterizations). Its behavior will thus be a reference for that of $(S_{53}A_{39})$-*b*-A_{133}.[28]

Diblock Dispersions. The $(S_{53}A_{39})$-*b*-A_{133} diblock films were powdered and dispersed all at a weight fraction $w_p = 0.05$ (i.e., 5 wt %) in deuterated water D_2O, at different pHs and ionic strengths. The pH of the dispersions was tuned via additions of sodium hydroxide (NaOH). With knowledge of the composition of the first block and of the diblock (namely, the overall acrylic acid content), appropriate amounts of NaOH were added so as to perform different values from 0 to 1, of the base-to-acid molar ratio

$$\alpha_{B/A} = n_{NaOH}/n_{AA} = n_{NaOH}/\left(n_{AA}^{(1)} + n_{AA}^{(2)}\right) \quad (1)$$

where n_{NaOH} is the number of moles of NaOH added, and $n_{AA} = n_{AA}^{(1)} + n_{AA}^{(2)}$ is the total number of acrylic acid functions from both the first statistical block $(S_{53}A_{39})$ and the second block A_{133}, with no distinction. This ratio will be referred to as "ionization" from now on. We cannot predict for now how the NaOH added will react with acrylic acid units from either block. As a result, we define the two alternative ionizations $\alpha_{B/A}^{(1)} \equiv n_{NaOH}/n_{AA}^{(1)}$ and $\alpha_{B/A}^{(2)} \equiv n_{NaOH}/n_{AA}^{(2)}$ pertaining to each block

$$\alpha_{B/A}^{(1)} = \left(1 + n_{AA}^{(2)}/n_{AA}^{(1)}\right)\alpha_{B/A} \quad (2)$$

$$\alpha_{B/A}^{(2)} = \left(1 + n_{AA}^{(1)}/n_{AA}^{(2)}\right)\alpha_{B/A} \quad (3)$$

where $n_{AA}^{(2)}/n_{AA}^{(1)} = (1 - w)/w\phi_{AA}$, $w = 0.465$ being the weight fraction of the first $(S_{53}A_{39})$ block in $(S_{53}A_{39})$-*b*-A_{133}, and $\phi_{AA} = 1/(1 + (1 - \varphi_{AA})M_S/\varphi_{AA}M_{AA}) = 0.33$ the weight fraction of acrylic acid in $(S_{53}A_{39})$, while $M_S = 104$ g/mol and $M_{AA} = 72$ g/mol are the molecular weights of styrene and acrylic acid segments, respectively. On the other hand, the ionic strength was tuned via additions of sodium chloride (NaCl). The concentration $c_S \equiv [Na^+] + [Cl^-]$ ranged from 0 to 6.0 mol/L (M).

All dispersions were stirred for 72 h and were allowed to equilibrate at room temperature for several days before undergoing SANS experiments. Depending on the values of $\alpha_{B/A}$ and c_S, the dispersion in water led to samples quite different in appearance, either biphasic or monophasic, whitish or transparent, gel-like, viscous, or liquid, as will be detailed when appropriate, in the Results section.

Monoblocks Dispersions. $(S_{53}A_{39})$ and A_{111} were also dispersed separately, both at a weight fraction 0.025 (i.e., 2.5 wt %) in heavy water, in the absence of salt. The two dispersions were then slowly titrated with a NaOH solution, and the pH was measured. On the other hand, a {47/53} mixture (in wt %) of the two separate polymers was dispersed in salt-free heavy water so that the overall polymer weight fraction was $2 \times 0.025 = 0.05$ (i.e., 5 wt %). This binary dispersion, equivalent (in terms of blocks molecular weight and blocks weight ratio) to the diblock $(S_{53}A_{39})$-*b*-A_{133} dispersions, was then slowly titrated.

pH Measurements. Potentiometric titrations were performed at 23 ± 1 °C, using a Bioblock Scientist pH meter on 2.5 wt % dispersions of monoblocks $(S_{53}A_{39})$ and A_{111} and on a 5 wt % dispersion of diblock $(S_{53}A_{39})$-*b*-A_{133}. A concentrated NaOH solution (3.5 M) was used so that the concentration at the end of the titration was close to the initial one to avoid concentration effects on the pH measurements. The apparatus was calibrated using 4.00 ± 0.01, 7.00 ± 0.01, and 10.00 ± 0.01 buffer solutions just before the titrations. During the titration, a resting time of 30 s to 10 min was allowed for full reaction of the acrylic acid functions with the added NaOH, before the pH measured was considered stable and accurate. Note that, for all biphasic dispersions, the upper and lower phases were not separated for the purpose.

Structural Characterizations Using Scattering and Imaging Techniques. SANS was used to identify the structures and spacings on the dispersions described above, all at room temperature. The experiments were performed on PAXE, at the Laboratoire Léon Brillouin (LLB, Laboratoire commun CEA-CNRS), Saclay, France. Incoherent (background) scattering was subtracted manually: after plotting $q^4I(q)$ vs q,[4] the data was fitted at large wave-vector q to a linear law, whose slope is considered equal to the incoherent scattering. Atomic force microscopy (AFM) was performed in tapping mode on deposits of selected diblock dispersions, made on freshly cleaved mica surfaces. One drop of a solution was dried at 40−50 °C for a few minutes in an oven and stored at the same temperature overnight before the AFM experiment was performed.

3. Results

A pH-Dependent Lyotropic Behavior. Let us first report on the main structural features of $(S_{53}A_{39})$-*b*-A_{133} dispersions when varying ionization. The most important result is that this SANS study allows identifying four different ordered phases in four different ionization regimes, demonstrating that these diblocks possess a pH-dependent lyotropic behavior. The different types of spectra and corresponding ionization regimes are shown in Figure 2 and detailed hereafter:

(i) $0 \leq \alpha_{B/A} \leq 0.27$ (cf. Figure 2a): the dispersions are milky, biphasic upon resting with a swollen diblock structure as the lower phase and excess water as the upper phase. In the lower q range, the SANS curves show a primary structure factor peak at a position q^*, followed by several peaks at q-to-q^* ratios 1:2:3, characteristic of the structure factor $S(q)$ of a well-ordered lamellar (L) phase. As ionization is increased, the position q^* of the first correlation peak is shifted to smaller q values, showing the progressive swelling of the phase. In this ionization range, we observe a Porod regime where the scattered intensity scales as $I(q) \propto q^{-4}$. By analogy with previous work carried out on the L phases of diblock S_{83}-*b*-A_{123}, this feature demonstrates that the lamellar core formed by the more hydrophobic $(S_{53}A_{39})$ block presents a sharp interface consistent with the strong segregation regime of PSAA-*b*-PAA diblocks in the melt state.[25,26] Note that an upturn is visible in the intensity scattered at very small q.

(ii) $0.33 \leq \alpha_{B/A} \leq 0.40$ (Figure 2b): the SANS curves show a primary structure factor peak at a position q^*, followed by

TABLE 1: Diblock Characteristics

sample	f_{PSAA}[a]	φ_{AA}[b]	M_n[c]	$N_{SAA}^{(1)}$[d] $N_S^{(1)}$	$N_{SAA}^{(1)}$[d] $N_{AA}^{(1)}$	$N_{AA}^{(2)}$[e]	d_M (nm)[f]	e_M (nm)[g]	h_M (nm)[h]	ξ_M^2 (nm^2)[i]
S_{83}-*b*-A_{123}	0.565	0	18 000	83	0	123	33.7	9.5	7.4	1.70
$(S_{53}A_{39})$-*b*-A_{133}	0.549	0.42	17 900	53	39	133	20.9	5.7	4.7	2.83

[a] Volume fraction of the first block in the diblock, computed from ^{1}H NMR data, using the density $d_{PS} = 1.05$ g/cm^3 of a pure PS homopolymer as that of the first block and $d_{PAA} = 1.47$ g/cm^3 as the density of the second block. [b] Molar fraction of AA in the PSAA statistical first block. [c] Diblock number-average molecular weight M_n in g/mol. [d] Total polymerization degree of the PSAA first block, comprising $N_S^{(1)}$ styrene units and $N_{AA}^{(1)}$ acrylic acid units. [e] Polymerization degree of the second PAA block. [f] Period $d_M = 2\pi/q^*$ of the L-phase in the melt state, from the position q* of the first correlation peak in the SAXS spectrum. [g] Half-thicknesses of the PSAA layers, computed using d_M and f_{PSAA}. [h] Half-thicknesses of the PAA layers, computed using d_M and f_{PSAA}. [i] Area per chain (i.e., inverse of the surface density σ_M) in the melt state.

additional peaks at q-to-q^* ratios obeying 1:2:3 indicative of a smectic order, as in the previous L phase. This secondary lamellar phase, denoted L′, differs from the previous L phase. Indeed, the dispersions are not biphasic but slightly turbid, monophasic gels. Second, in contrast with the SANS curves of the L phases, we successively observe q^{-2} and q^{-4} scalings in the scattered intensity (cf. Figure 2b, $\alpha_{B/A} = 0.40$), associated with the theoretical form factor[29,30] $P_L(q) \cong 1/q^2 \sin^2(qe_L')/q^2$ of a monodisperse lamella of thickness $2e_L'$, dense and homogeneous in terms of scattering length density.[31] Finally, note that the position of the correlation peak for $\alpha_{B/A} = 0.33$ is shifted compared to that of the last specimen $\alpha_{B/A} = 0.27$ identified as a L phase: this demonstrates an abrupt and significant shrinkage of the period (of order $\Delta d = d(\alpha_{B/A} = 0.27) - d(\alpha_{B/A} = 0.33) = 65.4 - 57.6 = 7.8$ nm) in this L-to-L′ transition.

(iii) $0.46 \leq \alpha_{B/A} \leq 0.54$ (Figure 2c): the dispersions are slightly turbid, monophasic viscous liquids; their SANS spectra show a unique structure factor peak. The SANS signature is interpreted as that of a spherical (S) phase with a liquidlike order. At larger q values, the Porod regime $I(q) \propto q^{-4}$ is still observed, demonstrating the resilience of a sharp interface in the scattering object, in spite of the morphological reorganization. Note that AFM experiments were carried out in tapping mode on the sample obtained after a 30-μL drop of the $(S_{53}A_{39})$-*b*-A_{133} dispersion at ionization $\alpha_{B/A} = 0.46$ was deposited on a freshly cleaved mica surface and rapidly dried at room temperature and confirmed, as can be seen on the Figure 3, the presence of spherical objects. A spherical phase, denoted S, is thus evidenced.

(iv) $\alpha_{B/A} = 0.64$ (Figure 2c): the dispersion becomes a low-viscosity, clear liquid. The corresponding SANS spectrum is virtually free of structure factor contribution, which demonstrates an absence of order. However, the diblock has not attained full solubility yet: although the scattering intensity is very low, a form factor contribution is still clearly observed, which the observation of a small Porod regime $I(q) \propto q^{-4}$ supports as well. This spherical phase, denoted S′, differs from the previous S phase. Apart from the viscosity drop and the obvious absence of structure factor peak, the most dramatic effect observed with the S′ phase is the drop in the scattered intensity. The latter is much smaller than those of the last S phase ($\alpha_{B/A} = 0.46$) since a factor of 2−10 is found on the whole q range between the two dispersions, although both are homogeneous and have the same polymer concentration. Note that, in the same way, we find a factor of 10−50 between the intensities scattered by the S′ and the L′ phases of Figure 2b.

The symmetrical $(S_{53}A_{39})$-*b*-A_{133} diblock therefore forms objects with morphologies and long-range order that depend on ionization. Let us now recall the results obtained on diblock S_{83}-*b*-A_{123} previously reported on. When dispersed in water, the melt-state lamellar phase of this amphiphilic diblock copolymer forms lamellar objects presenting a smectic order. These core−shell objects comprise (i) a water-free lamellar PS core and (ii) a {PA, Na+} polyelectrolyte brush swollen with water. The lamellar PS core, of constant half-thickness 8.5 nm, was always found of the same shape and size than those of the initial melt state regardless of concentration, ionization, or ionic strength. The same was found for diblocks of different symmetries, such as S_{20}-*b*-A_{208} and S_{43}-*b*-A_{163}, which, respectively, form spherical[32] and cylindrical phases[6] in the melt state. Upon dispersion, these phases produce spherical or cylindrical core−shell objects, whose PS cores have exactly the same shape and size as those of the initial melt state.

Our understanding is that shape reorganizations in PS-*b*-PAA structures are forbidden when the PS cores are glassy at room temperature. The objects found in PS-*b*-PAA dispersions are simply reminiscent of the structures formed in the initial melt, used in the dispersions. For this reason, PS-*b*-PAA structures are considered as frozen-in. If no heating is applied, there is no way for the structure to reorganize or to present morphological transitions upon dilution. On the contrary, when the constraint of glassiness is released by annealing at high temperature, PS-*b*-PAA structures undergo morphological transitions.[6]

In Figure 4, we compare, as a function of ionization $\alpha_{B/A}$, the spacings $d \equiv 2\pi/q^*$ of the structures formed by $(S_{53}A_{39})$-*b*-A_{133} and S_{83}-*b*-A_{123} in salt-free conditions. While S_{83}-*b*-A_{123} always presents frozen-in L- phases, with a swelling increasing monotonically with ionization, the spacing in the $(S_{53}A_{39})$-*b*-A_{133} dispersions repeatedly deviates from that of S_{83}-*b*-A_{123} as different phases are identified: the discontinuities coincide with L-to-L′, L′-to-S, and S-to-S′ transitions. Because it presents morphological transitions at room temperature, the behavior of $(S_{53}A_{39})$-*b*-A_{133} is thus drastically different from that of S_{83}-*b*-A_{123}: the presence of AA segments in the first block suppresses the frozen-in nature of the diblock at certain pH values.

The loci of the different structural transitions are in fact linked to specific ionizations of the two constitutive blocks. We have investigated separately the ionizations of the $(S_{53}A_{39})$ first block and of A_{111}, a homopolymer approximately equivalent to the second block of $(S_{53}A_{39})$-*b*-A_{133}. Figure 5 shows the titration curves of $(S_{53}A_{39})$ and A_{111} as a function of their ionization. We extract from these titration curves (cf. Appendix A) the apparent pK_A of these two polyacids: we find 5.4 for A_{111} and 8.2 for $(S_{53}A_{39})$. The ionization of $(S_{53}A_{39})$, hence its solubility, would certainly be affected by the presence of a stronger polyelectrolyte, such as A_{111}, and it seemed profitable to investigate a binary mixture. Figure 5 also shows the titration curve of the two polyacids as a {47/53} binary mixture denoted $(S_{53}A_{39})/A_{111}$: the titration curve of the mixture perfectly superimpose with that of A_{111} alone on the range $0 \leq \alpha_{B/A} \leq 0.23$, i.e., as long as pH ≤ 4.9. In this ionization range, the pH

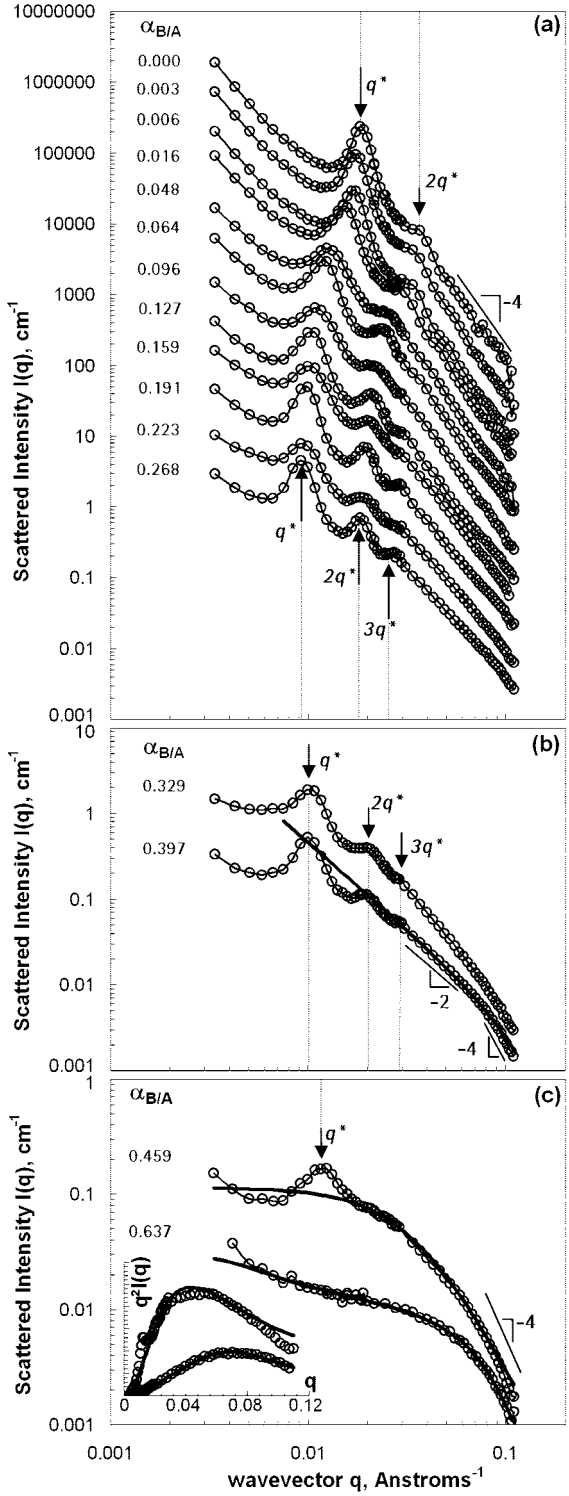

Figure 2. SANS spectra of the $(S_{53}A_{39})$-*b*-A_{133} diblock structures of increasing ionization in salt-free conditions. (a) Scattered intensities $I(q)$ vs q at different ionizations $\alpha_{B/A}$, as indicated. The curves were multiplied by powers of 3 for the sake of clarity. (b) Same as in part a for two larger ionizations. The line is a fit to the large q window ($q \geq 0.03$ Å^{-1}) according to the theoretical form factor of a dense lamellae of half thickness $e_{L'} = 1.3$ nm. (c) Same as in part b for two even larger ionizations. The lines are fit on the whole q window according to the theoretical form factor of a core−shell spherical object. Insert: corresponding Kratky plots $q^2I(q)$ vs q. In all three figures, the position q^* of the first structure peak is indicated along with the higher orders of reflection when present.

is thus imposed by the pure poly(acrylic acid) block A_{111}, while $(S_{53}A_{39})$ has no role whatsoever. When the pH of the mixture

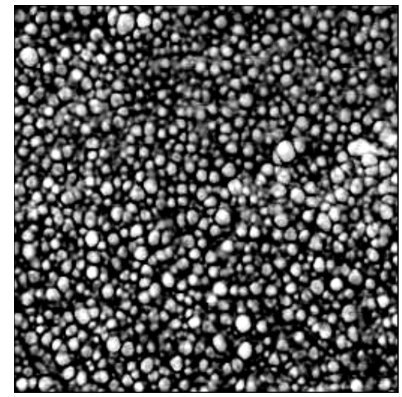

Figure 3. 1-μm^2 AFM picture, carried out in tapping mode on a drop of a dispersion of diblock $(S_{53}A_{39})$-*b*-A_{133} at an overall ionization $\alpha_{B/A} = 0.46$, in the absence of salt, dried on a freshly cleaved mica surface.

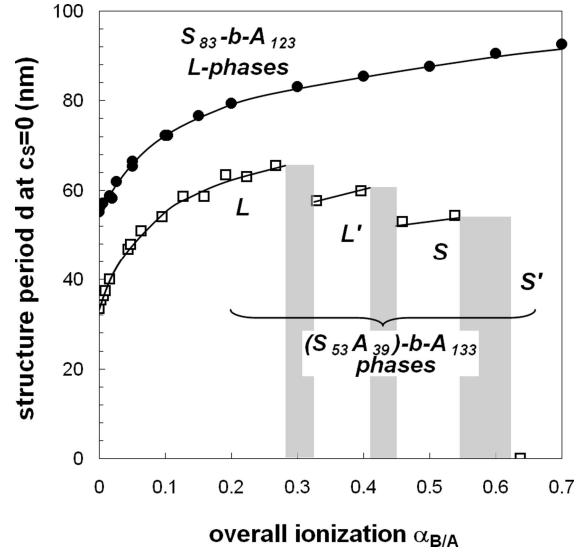

Figure 4. Evolution of the structure period $d = 2\pi/q^*$, as a function of the overall ionization $\alpha_{B/A}$ in salt-free conditions, for diblocks $(S_{53}A_{39})$-*b*-A_{133} (□) and S_{83}-*b*-A_{123} (●). L is a frozen-in lamellar phase, L′ a molten lamellar phase, S a spherical phase, and S′ a state where a scattering object exists yet no long-range order is observed. The lines are guide for the eye. Data on S_{83}-*b*-A_{123} are taken from ref 27.

reaches 4.9, at an overall ionization of $\alpha_{B/A} = 0.23$, the titration curve of the binary mixture starts departing from that of A_{111}, which we associated with the beginning of the ionization of $(S_{53}A_{39})$. It is not fortuitous that this also coincides with the first morphological transition (from L to L′), as will be detailed in the Discussion section. For now, our understanding is that, as water together with charges start penetrating the $(S_{53}A_{39})$ lamellar core, the core melts and can now undergo structural transitions. The control of the pH of the solution therefore triggers the transition from a glassy to a molten core.

Finally, Figure 5 shows the titration curve of the diblock, that is, when the two polyacids are covalently linked through the diblock architecture. We observe that the values of the apparent pK_A are barely modified (cf. Appendix A), even though the titrations of the $(S_{53}A_{39})$-*b*-A_{133} diblock and of its equivalent binary mixture $(S_{53}A_{39})/A_{111}$ do not exactly superimpose.[33] For $\alpha_{B/A} \leq 0.66$ (pH ≤ 7.0), the pH of $(S_{53}A_{39})$-*b*-A_{133} is larger than that of $(S_{53}A_{39})/A_{111}$ yet becomes smaller for $\alpha_{B/A} \geq 0.66$ (pH ≥ 7.0): a second critical ionization $\alpha_{B/A} = 0.66$ (pH = 7.0) is then defined. The topological link in the diblock architecture obviously affects the competition for ionization between the two blocks.

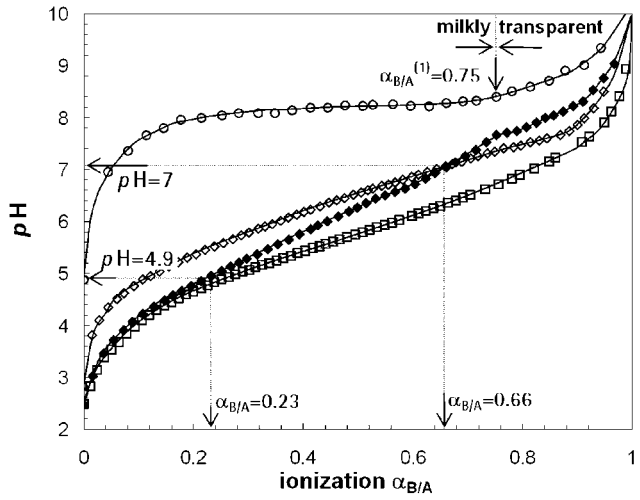

Figure 5. pH as a function of ionization of salt-free dispersions of $(S_{53}A_{39})$ (○), A_{111} (□), diblock $(S_{53}A_{39})$-*b*-A_{133} (◇), and its equivalent {47/53} binary mixture $(S_{53}A_{39})/A_{111}$ (◆).

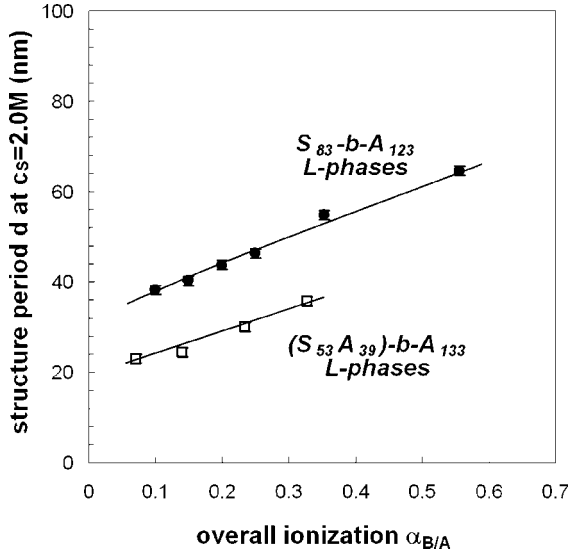

Figure 6. Evolution of the structure period $d = 2\pi/q^*$ as a function of the overall diblock ionization $\alpha_{B/A}$ at ionic strength $c_S = 2.0$ mol/L for diblocks $(S_{53}A_{39})$-*b*-A_{133} (□) and S_{83}-*b*-A_{123} (●). L phases are observed for both systems on the ionization range investigated. In both figures, the lines are guide for the eye. Data on S_{83}-*b*-A_{123} are taken from ref 27.

Again, it is not fortuitous that all the structural transitions of $(S_{53}A_{39})$-*b*-A_{133} occur in between two critical pH values. The transition from L′ to S phases, in particular, occurs around pH = 5.8 ($\alpha_{B/A} \approx 0.30$ according to the titration curve of the diblock), a second value which will prove useful in the next paragraph.

A Salt-Dependent Lyotropic Behavior. We now investigate the effect of the ionic strength on the structural behavior. As an example, Figure 6 shows the evolution of the structure spacing *d* with $\alpha_{B/A}$, at a salt concentration $c_S = 2.0$ mol/L. In this salty case, $(S_{53}A_{39})$-*b*-A_{133} then shows no morphological transition anymore. The dispersions only present L phases on the whole ionization range, including the point $\alpha_{B/A} = 0.33$, which consisted in a L′ phase in the absence of salt. The behavior of $(S_{53}A_{39})$-*b*-A_{133} then strongly resembles that of S_{83}-*b*-A_{123}. Changing the ionic strength is thus another way to tune the lyotropic behavior of $(S_{53}A_{39})$-*b*-A_{133}. However, the effects of ionization and ionic strength are not independent. We detail the structural behavior as c_S is increased from 0 to 6.15 M, for three particular ionizations corresponding to three different phases in salt-free conditions, i.e., a L phase at $\alpha_{B/A} = 0.17$, L′ phase at $\alpha_{B/A} = 0.33$, and a S phase at $\alpha_{B/A} = 0.46$.

(i) in the L-phase region, i.e., $\alpha_{B/A} = 0.17$ (Figure 7a): on the whole range of added salt, the dispersions are milky and biphasic upon resting very much like the salt-free L phase; all SANS curves show lamellar patterns with the upturn in the intensity scattered at small *q* characteristic of L phases. As c_S is increased, the position q^* of the first correlation peak significantly increases. This implies a decrease in the lamellar spacing *d*, due to an osmotic compression effect already seen in the reference L phases of S_{83}-*b*-A_{123}. We conclude that a L phase is conserved on the whole salt concentration range investigated and that salt simply makes the period of this L phase shrink.

(ii) In the L′-phase region, i.e., $\alpha_{B/A} = 0.33$ (Figure 7b): for $0 \le c_S \le 3.4 \times 10^{-4}$ M, the dispersions are monophasic transparent gels, and the SANS signature of the L′ phase seems conserved. For 3.4×10^{-3} M $\le c_S \le 3.4 \times 10^{-2}$ M, the dispersions become milky but are still monophasic. For $c_S \ge 3.4 \times 10^{-1}$ M, the dispersions become biphasic upon resting, with a bottom white phase and an upper transparent phase of excess water, very much like L phases. The upturn in the intensity scattered at small *q* characteristic of L phases appears when $c_S \ge 3.4 \times 10^{-1}$ M, while this feature is not observed up to $c_S = 3.4 \times 10^{-2}$ M. We conclude that L′ phases are conserved for at least $c_S \le 3.4 \times 10^{-4}$ M and that L phases are obtained when $c_S \ge 3.4 \times 10^{-1}$ M.

(iii) In the S-phase region, i.e., $\alpha_{B/A} = 0.46$ (Figure 7c): up to $c_S = 3.4 \times 10^{-2}$ M, the dispersions are turbid viscous liquids, and their SANS signature remains that of an S phase, the three curves looking very much alike. The position of the unique broad structure peak, in particular, remains the same. For $c_S \ge 3.4 \times 10^{-1}$ M, the SANS spectra resemble lamellar patterns, showing a narrower first-order structure peak and a growing second-order one. Although it is difficult for now to establish which of the L or L′ phases is in fact obtained, we notice both q^{-2} and q^{-4} dependences originating from the lamellar form factor, which only the L′ phase showed in the absence of salt. Their fit leads to bilayer thicknesses of the order 1.6−2.1 nm, of the same order as those of the salt-free L′ phases (1.3−1.8 nm). It appears that a critical salt concentration of the order 3.4×10^{-2} to 3.4×10^{-1} M separates the regime of a stable S phase from that where the L′ phase is obtained.

Therefore, the morphology and long-range order of the phases of $(S_{53}A_{39})$-*b*-A_{133} in water also depend on the ionic strength. In conclusion, $(S_{53}A_{39})$-*b*-A_{133} presents a pH- and salt-dependent lyotropic behavior, as represented in the phase diagram of Figure 8. The two experimental parameters allow morphological changes to occur, although the polymer concentration was kept constant. Since diblock $(S_{11}A_{12})$-*b*-A_{229}, the asymmetric analogue of $(S_{53}A_{39})$-*b*-A_{133}, was shown to present spherical micelles of concentration-dependent aggregation number when dispersed in water,[32] we expect the phase diagram of $(S_{53}A_{39})$-*b*-A_{133} to depend on diblock concentration as well. However, in the present study, the concentration was not varied, so as to focus on the pH- and salt-dependent effects.

As before, the locii $\{\alpha_{B/A}, c_S\}$ of the different structural transitions must be somewhat linked to specific ionizations of the two constitutive blocks in the presence of salt. Figure 9 shows the evolution of the pH of dispersions of $(S_{53}A_{39})$-*b*-A_{133} as a function of c_S, while $\alpha_{B/A}$ was this time kept constant. We adopted the two starting pH values of 5.8 and 6.2, respectively, corresponding to the L′ phase at $\alpha_{B/A} = 0.33$ and

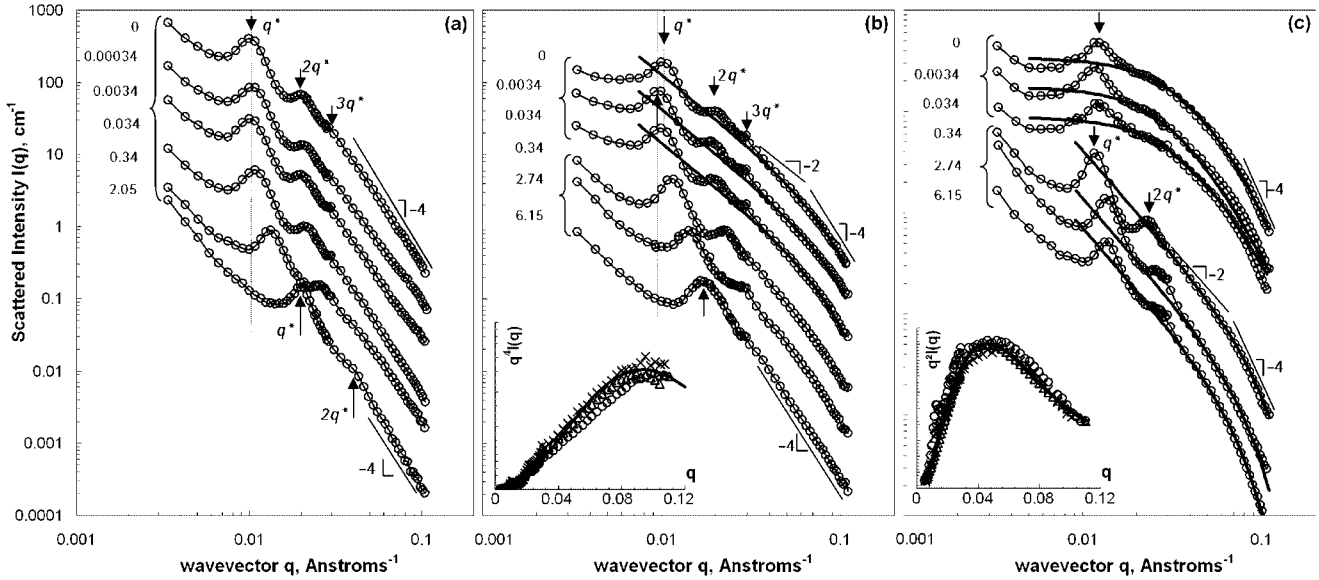

Figure 7. SANS spectra of the $(S_{53}A_{39})$-*b*-A_{133} diblock structures of increasing ionization in the presence of salt. (a) Scattered intensities $I(q)$ vs q at $\alpha_{B/A} = 0.17$ for an increasing salt concentration c_S as indicated. (b) Same as in part a, $\alpha_{B/A} = 0.33$. For the three top curves ($c_S \leq 0.034$ M), the lines are fits to the large q window ($q \geq 0.03$ Å^{-1}) according to the theoretical form factor of a dense lamellae of half-thickness 1.6 nm in all cases. Insert: Porod plots $q^4I(q)$ vs q associated with the curves in part b, showing the superimposition in the large q window. (c) Same as in part b, $\alpha_{B/A} = 0.46$. For the three top curves ($c_S \leq 0.034$ M), the lines are fits to the large q window according to the theoretical form factor of an object comprising a core and a shell, both swollen with water. The core is found of radius 2.2 ± 0.05 nm in all cases. For the three bottom curves ($c_S \geq 0.34$ M), the lines are fits to the large q-window ($q \geq 0.03$ Å^{-1}), according to the theoretical form factor of dense lamellae of half-thickness 1.6, 1.9, and 2.1 ± 0.05 nm. Insert: Kratky plots $q^2I(q)$ vs q associated with the three top curves in part c, showing superimposition in the large q window. In all figures, the curves have been vertically shifted for the sake of clarity. In all three figures, the position q^* of the first structure peak is indicated along with the higher orders of reflection when present.

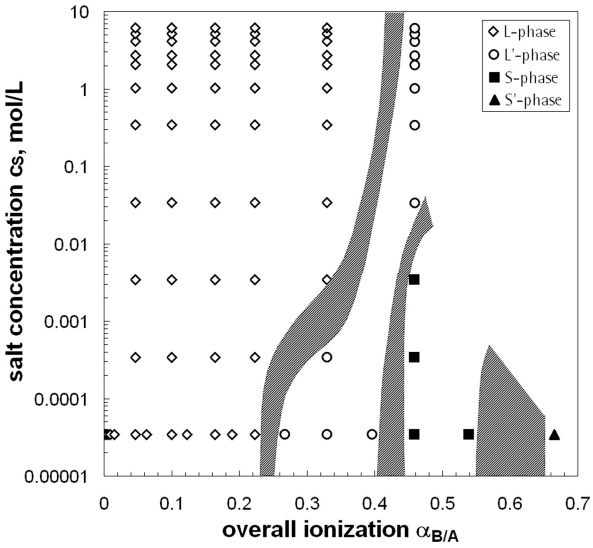

Figure 8. Phase diagram showing the lyotropic behavior of diblock $(S_{53}A_{39})$-*b*-A_{133} with ionization and salt concentration, at constant polymer concentration $w_p = 0.05$.

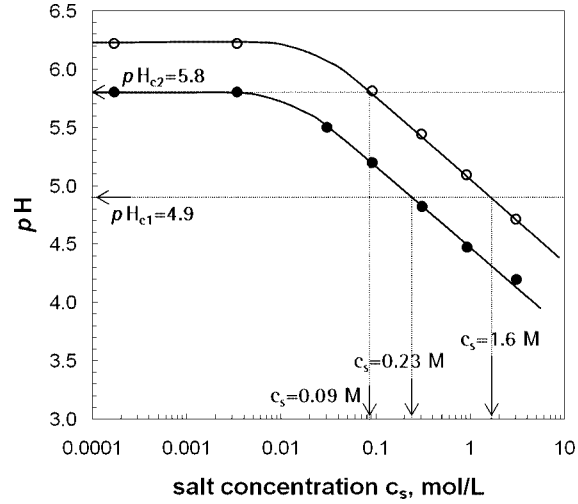

Figure 9. pH of dispersions of $(S_{53}A_{39})$-*b*-A_{133} as a function of salt concentration c_S at constant ionizations $\alpha_{B/A} = 0.33$ (●) and 0.46 (○) with starting pH values of 5.8 and 6.2 when in salt-free conditions, respectively.

to the S-phase at $\alpha_{B/A} = 0.46$ in salt-free conditions. We indicate the critical salt concentrations where the pH of the dispersions crosses the two critical values: (i) $pH_{c1} = 4.9$, where the ionization of $(S_{53}A_{39})$ begins, and (ii) $pH_{c1} = 5.8$, which corresponds to the transition from L′ to S phases ($\alpha_{B/A} \approx 0.30$) according to the titration curve of the diblock. The pH of the L′ phase decreases as c_S is increased and crosses $pH_{c1} = 4.9$ when $c_S = 2.3 \times 10^{-1}$ M, which indeed falls in the range 3.4×10^{-2} to 3.4×10^{-1} M identified thanks to SANS.[35] In the same way, the pH of the S-phase decreases as salt concentration is increased and crosses $pH_{c1} = 5.8$ when $c_S = 0.9 \times 10^{-2}$, which again falls in the range 3.4×10^{-2} to 3.4×10^{-1} M, identified thanks to SANS. Therefore, the added salt decreases the pH so that the dispersion may cross back the critical pH values where structural transitions occur: pH and ionic strength have opposite effects. This fully explains why the transitions from L to L′ or from L′ to S phases are shifted to higher ionization when salt is added. In the following Discussion section, we detail separately the physics of each microphase identified.

4. Discussion

Low Ionization Regime: Glassy, Frozen-In L Phases. The existence of a long-range order and well-defined elementary

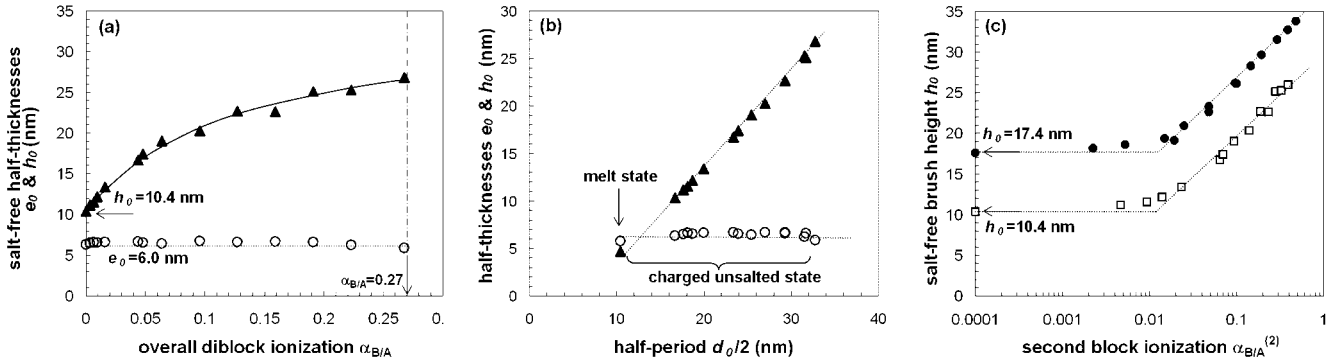

Figure 10. (a) Half-thicknesses e_0 (○) and h_0 (▲) vs the overall ionization $\alpha_{B/A}$ in the absence of added salt; the arrows indicate the asymptotic uncharged unsalted state where $e_0 = 6.0$ nm and $h_0 = 10.4$ nm. (b) Data replotted from part a as a function of the L-phase half period $d_0/2$ on the $\alpha_{B/A}$ range investigated. The arrow indicates the values $e_M = 5.7$ nm and $h_M = 4.7$ nm of the initial melt state. (c) Half-thicknesses h_0 vs the second block bare ionization $\alpha_{B/A}^{(2)}$ in the absence of added salt, for the two lamellar phases formed by S_{83}-*b*-A_{123} (○) and ($S_{53}A_{39}$)-*b*-A_{133} (▲). The lines are guides for the eye, which define the two regimes observed on either side of the threshold value $\alpha_{B/A}^{(2)} = 0.015$. The arrows indicate the asymptotic value h_0 in the "uncharged unsalted case", namely, $h_0 = 17.4$ nm for S_{83}-*b*-A_{123} and 10.4 nm for ($S_{53}A_{39}$)-*b*-A_{133}.

objects in water allows modeling the structure and form factor contributions to the scattering intensity. For L phases, lamellar period and domains thicknesses can be extracted from the position q^* of the first structure peak and from the relative height of the structure peaks. This helpful and reliable method to determine the core and brush thicknesses is detailed in Appendix B. We discuss the results below.

In the salt-free case, where only ionization was varied, Figure 10a shows the half-thicknesses of the ($S_{53}A_{39}$) and A_{133} sublayers, respectively, denoted e_0 and h_0, as a function of $\alpha_{B/A}$ on the range $0 \leq \alpha_{B/A} \leq 0.27$ where L phases were identified. While e_0 is nearly constant (6.0 ± 0.5 nm), regardless of $\alpha_{B/A}$, h_0 increases from 10.4 to 26.0 nm. In Figure 10b, e_0 and h_0 are shown as a function of the half-period d_0 of the L phase: h_0 increases linearly with $d_0/2$. The data extrapolates well to the half-thickness $h_M = 4.7$ nm of the A_{133} sublayer measured in the initial melt state (cf. the arrow in Figure 10b). Therefore, as ionization is increased, the swelling of the entire L phase solely results from the swelling of the A_{133} sublayer, while the ($S_{53}A_{39}$) one remains frozen-in and unable to reorganize. This behavior resembles that of the pure PS lamellar core formed by the hydrophobic block of S_{83}-*b*-A_{123}. The titrations presented in the Results section suggest that, in the ionization range $0 \leq \alpha_{B/A} \leq 0.27$, only A_{133} reacts with the NaOH introduced, while the acrylic acid functions of ($S_{53}A_{39}$) remain protonated. Consequently, the overall diblock ionization $\alpha_{B/A}$ must be replaced with the ionization $\alpha_{B/A}^{(2)}$ pertaining to A_{133} only. Figure 10c now shows the evolution of h_0 as a function of $\alpha_{B/A}^{(2)}$. When superimposing the data obtained for S_{83}-*b*-A_{123} in our previous work,[27] it becomes obvious that the L phases of these two diblocks behave very similarly. More precisely, in salt-free conditions, two ionization regimes can be distinguished concerning the evolution of the poly(acrylic acid) brush height in S_{83}-*b*-A_{123} and ($S_{53}A_{39}$)-*b*-A_{133} L phases:

(i) For low enough ionizations, i.e., $\alpha_{B/A}^{(2)} \leq 0.015$, h_0 is constant and equal to the value at zero ionization, $\alpha_{B/A}^{(2)} = 0$, namely, $h_0 = 10.4$ nm for ($S_{53}A_{39}$)-*b*-A_{133} and $h_0 = 17.4$ nm for S_{83}-*b*-A_{123}.

(ii) For $\alpha_{B/A}^{(2)} \geq 0.015$, h_0 increases from 10.4 to 26.0 nm for ($S_{53}A_{39}$)-*b*-A_{133} and from 17.6 to 33.8 nm for S_{83}-*b*-A_{123}.

On the other hand, in the presence of monovalent salts such as NaCl, the brush height presents characteristic regimes, which we give evidence of in the following. We now extract the half thicknesses of the ($S_{53}A_{39}$) and A_{133} sublayers, respectively, denoted e and h, when ionization as well as salt content are varied, on ranges $0 \leq \alpha_{B/A} \leq 0.27$ and $0 \leq c_S \leq 6.0$, where only L phases have been identified with ($S_{53}A_{39}$)-*b*-A_{133}. In Figure 11a, we plot the evolution of e and h as a function of the half period $d/2$. As before, we observe that e is approximately constant, equal to 5.8 ± 0.5 nm, which is again close to the value $e_M = 5.7$ nm of the initial melt state. On the other hand, h increases again linearly with the L-phase half period $d/2$, from 6.7 up to 25.7 nm. We conclude that within the ionization range $0 \leq \alpha_{B/A} \leq 0.27$, the ($S_{53}A_{39}$) core can be considered in the presence of salt as frozen-in and replace again the overall ionization $\alpha_{B/A}$ with the ionization $\alpha_{B/A}^{(2)}$ pertaining to the second block only. Values $\alpha_{B/A} = 0.032$, 0.10, 0.16, and 0.22 correspond to $\alpha_{B/A}^{(2)} = 0.048$, 0.14, 0.23, and 0.33, respectively. Figure 11b shows the evolution of the A_{133} domain half thickness h as a function of c_S, for the four different values of $\alpha_{B/A}^{(2)}$. We observe that h follows a two-regime behavior. Defining c_S^* as the threshold value between the two regimes, we find that:

(iii) For $c_S \leq c_S^*$, h is approximately constant with c_S, equal to the value h_0 in the "charged salt-free state"; moreover, the more ionized the diblock, the larger the value of h, at a given salt concentration.

(iv) For $c_S \geq c_S^*$, h decreases as $c_S^{-\gamma}$, with an experimental exponent γ verifying $0.29 \leq \gamma \leq 0.31$; moreover, the more ionized the diblock, the larger the value of h, at a given salt concentration.

As was shown for S_{83}-*b*-A_{123}, frozen-in L phases can constitute model flat dense polyelectrolyte brushes. The free energy of a flat polyelectrolyte brush (per polyelectrolyte chain) reads $F_{brush} = F_{el,brush} + F_m + F_{ci}$,[17,18] where (i) $F_{el,brush}/k_BT = h^2/N_2a^2$ is the attractive entropic contribution resulting from the stretching of a polyelectrolyte chain comprising N_2 motives; (ii) $F_m/k_BT = [{}^1/_2\tau c_2^2 + {}^1/_6a^3\omega c_2^3 + \ldots]a^3h\xi_L^{-2}$ is the virial-like contribution associated with the monomers free energy of mixing in the brush, τ and ω being the adimensional 2- and 3-body cluster integrals and $c_2 = N_2/h\xi_L^2$ the monomer concentration in the brush; and (iii) $F_{ci} = h\xi^2(fc_2 + c_S)\ln(fc_2 + c_S) - h\xi^2c_S\ln(c_S)$ introduced by Csajka et al.[19] is the repulsive entropic contribution associated with the free energy of mixing of the counterions confined inside the polyelectrolyte brush at a salt of concentration c_S, f being the charge fraction, ξ_L^2 the area per chain, and fc_2 the counterions concentration in the brush. The last contribution yields $F_{ci,salt\text{-}free} \cong fN_2 \ln c_2$ in salt-free conditions, $fc_2 \gg c_S$ and $F_{ci,salty} \cong fN_2[1 + \ln c_S + fN_2/2h\xi^2c_S]$ in highly salty ones, $fc_2 \ll c_S$. For intermediate salt concentra-

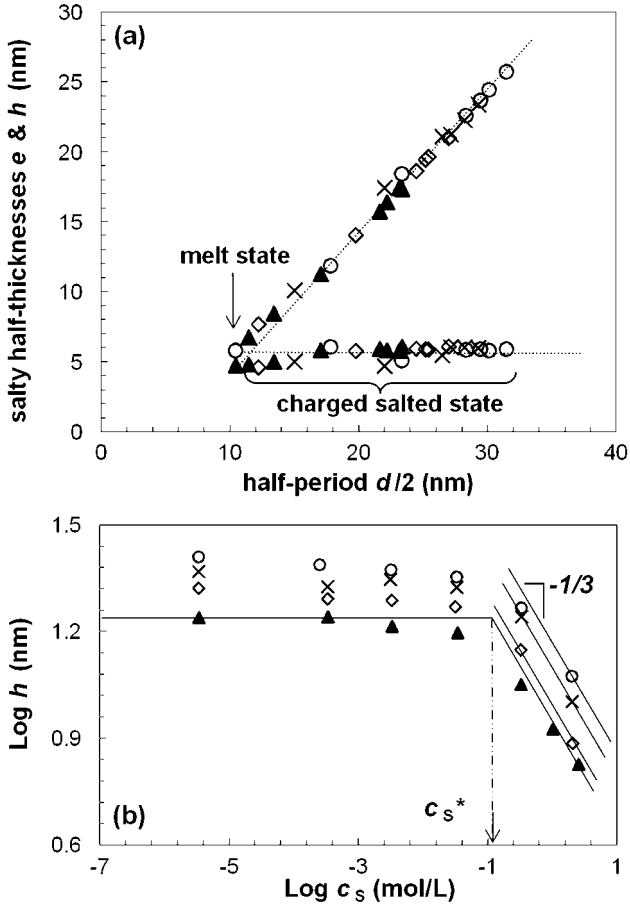

Figure 11. (a) Half thicknesses e and h vs the L-phase half period $d/2$ for the different salt concentrations and the four different ionization values $\alpha_{B/A}$ investigated, i.e., 0.05 (▲), 0.10 (◇), 0.17 (×), and 0.24 (○). The arrow indicates the values $e_M = 5.7$ nm and $h_M = 4.7$ nm measured in the initial melt state. (b) Half thickness h vs salt concentration c_S in logarithmic scales for the four corresponding values of second-block ionization $\alpha_{B/A}^{(2)}$: 0.048 (▲), 0.14 (◇), 0.23 (×), and 0.33 (○). The full lines are guides for the eye and define the two regimes observed on either side of the threshold concentration c_S^*. In the salty domain, $c_S > c_S^*$, a scaling $h \propto c_S^{-1/3}$ is observed. In both domains, h increases with $\alpha_{B/A}^{(2)}$.

tions, only the original expression applies, as neither fc_2 nor c_S can be neglected.

Minimizing F_{brush} with respect to h leads to several predictions for the evolution of the brush height at equilibrium. In the absence of salt, the two regimes observed experimentally and shown in Figure 11a simply correspond to the well-known regimes of neutral and osmotic brush (respectively, denoted NB and OsB), where the attractive contribution of the chain stretching is balanced either with the repulsive monomer virial contribution when ionization is small or with that of the counterions when ionization is significant. On the other hand, the two regimes observed in Figure 11b are expected from an osmotic polyelectrolyte brush of constant surface density in the presence of salt: the first domain $c_S \leq c_S^*$, where h is constant with c_S, corresponds to the salt-free osmotic brush (OsB), while the second domain $c_S \geq c_S^*$ corresponds to the salty (SB) regime. In particular, in this latter regime, the brush height is expected to follow

$$h = N_2 a f^{2/3} (a\xi_L^2)^{-1/3} c_S^{-1/3} \quad (4)$$

as predicted by several mean-field studies.[17,18] The threshold salt concentration $c_S^* \equiv fN_2/h\xi_L^2$, defined as the locus of the transition from low- to high-salt regimes, is then exactly equal to the concentration of Na^+ counterions confined inside the brush: in simple terms, c_S^* corresponds to the minimum amount of salt needed to overcome the counterions osmotic pressure inside the bush. Beyond c_S^*, the salt starts compressing the brush according to the well-known scaling law $h \propto c_S^{-1/3}$, which was verified in numerous experimental cases, including our own previous work on the model polyelectrolyte brush provided by the L phases of S_{83}-b-A_{123}.[27] Here, for the polyelectrolyte brush provided by the L phases of $(S_{53}A_{39})$-b-A_{133}, we find scaling exponents $0.29 \leq \gamma \leq 0.31$ regardless of the ionization, which agree well with the prediction of eq 4. We stress that the $c_S^{-1/3}$ scaling is a consequence of the frozen nature of the bilayers formed by $(S_{53}A_{39})$-b-A_{133}, as it can only be observed if the area per chain ξ_L^2 is constant throughout the whole experiment.

Finally, the SANS experiments show that the dispersions found in the low ionization regime $0 \leq \alpha_{B/A} \leq 0$ consist in lamellar phases comprising a frozen glassy hydrophobic core and a flat, osmotic polyelectrolyte brush. The A_{133} polyelectrolyte blocks are tethered to a substrate, i.e., the $(S_{53}A_{39})$ core, of constant curvature and constant surface density. Their behavior with ionization and salt confirm previous results on other frozen-in lamellar phases of PS-b-PAA diblocks.

Finally, we point out that in the mean-field description of the core-brush structures formed by the self-assembly of amphiphilic diblocks, additional contributions such as core chains stretching and core/water interfacial cost, are omitted simply because the core is frozen-in: a change in surface density being impossible, these contributions are irrelevant for the minimization of the total free energy, hence, in the polyelectrolyte brush height resulting from the balances between the different contributions. This point, however, will prove crucial in the next paragraph dedicated to the L′ phase, where the energetics of the nonfrozen core are detailed.

Intermediate Ionization: Elucidating the Morphological Transition from L to L′. Once the ionization of $(S_{53}A_{39})$ begins for $\alpha_{B/A} \geq 0.27$, the transition to the second lamellar structure L′ is observed. The transition is characterized by two features: (i) a sudden drop in the smectic period $\Delta d = 7.8$nm and (ii) a bilayer half thickness $e_{L'} = 1.3$ nm estimated from the form factor fitting (cf. Figure 2b), significantly smaller than that of $e_{L'} = 6.0 \pm 0.5$ nm in the L phase. We notice that the drop $\Delta 2e = 2(e_L - e_{L'}) = 2 \times (5.7 - 1.3) = 8.8$ nm in bilayer thickness is rather close to that in smectic period $\Delta d = 7.8$ nm measured experimentally. The drop in period which characterizes the L to L′ transition therefore results from the thinning of the lamellar core, while the brush height appears roughly constant. Estimating the Gaussian size of a $(S_{53}A_{39})$ block to $aN_1^{1/2} \approx 5.4$ nm (given $N_1 = 92$ motives and a size $a^3 = 0.165$ nm^3 with the styrene motive as the reference unit volume), the core blocks are only slightly stretched in the L phase and are somewhat compressed in the L′ phase.

The thinning of the lamellar core therefore results in an increase of the area per chain, as schematically represented in Figure 12. This characteristic feature of the L to L′ transition can be understood from a thermodynamic standpoint. Indeed, the total free energy $F_{L'} = F_{brush} + F_{core}$ (per diblock chain) of a L′ phase is the sum of a brush contribution $F_{brush} \approx F_{el,brush} + F_{ci}$ identical to that of the previous paragraph (restricting ourselves to the range of significant enough ionizations, where the virial-like monomer contribution F_m is negligible) and of a core contribution $F_{core} = F_{el,core} + F_\gamma$, where $F_{el,core} = e^2/N_1a^2$ and $F_\gamma/k_BT = \gamma\xi_{L'}^2$ (both expressed per core chain), respectively, correspond to the entropic contribution related to the elastic

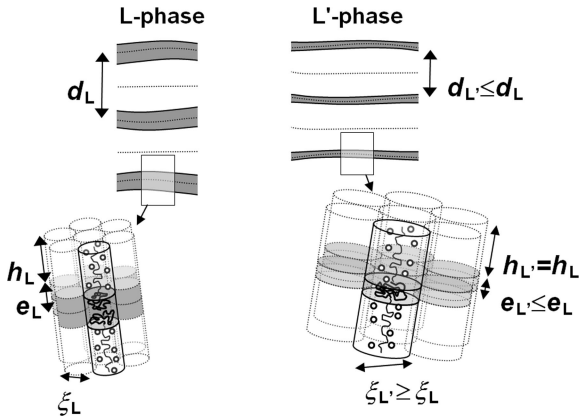

Figure 12. Schematic illustrations of the L and L′ phases, respectively, identified in the low and intermediate ionization ranges. The close ups detail the structural change inferred from the decrease in lamellar period: the transition from L to L′ results in a thinning of the bilayer and, thus, in an increase of the surface per chain, the height h of the neat PAA brush remaining unaffected as expected for osmotic brushes (see text).

deformation of the core blocks and to the enthalpic contribution associated with the interfacial tension γ between the ($S_{53}A_{39}$) core and the swollen brush. While the minimization of $F_{L'}$ must be done with respect to the independent variables e and h, we point out that minimizing $F_{L'}$ with respect to h in salt-free conditions, leads to

$$\left(\frac{\partial F_{L'}}{\partial h}\right)_e \equiv \left(\frac{\partial F_{\text{brush}}}{\partial h}\right)_e = \frac{h}{N_2 a^2} - \frac{fN_2}{h} = 0 \qquad (5)$$

and to the classical prediction $h \cong N_2 a f^{1/2}$. The latter, as expected, does not depend on the core energetics and, in particular, on the area per chain, as pointed out in the previous section dedicated to the L phase. We can therefore understand that the change in smectic period Δd measured experimentally is solely due to a change in bilayer half-thickness $\Delta 2e$: the concomitant change in surface density does not affect the height of the osmotic brush.

Our understanding of the transition is as follows: as soon as very few molecules of water enter the core, the latter undergoes a transition from glassy to molten, thus relieving the constraint of constant brush surface density. The area per chain can adapt: it increases as a result of the pressure imposed by the counterions cloud confined inside the brush, although this happens at the expense of a core/water interfacial cost and possibly, a slight compression of the core blocks, while the stretching contribution of the brush blocks remains unaffected, since its energetics is independent of brush density.

We consider that the fraction φ of water that has penetrated the core upon the transition can be neglected at first. In fact, as the titration of block ($S_{53}A_{39}$) alone showed, the block remains mostly insoluble in water, producing milky dispersions which become biphasic upon resting. The core could very well remain water-free in the process. As a result, the area per chain and the core half thickness are bound by the condition of conservation of matter $N_1 a^3 = e\xi_{L'}^2(1 - \varphi) \cong e\xi_{L'}^2$. Schematically, our transition scenario suggests that the entropy gained by the counterion cloud as the brush becomes less dense, from $1/\xi_L^2$ to $1/\xi_{L'}^2$, should correspond to the enthalpic cost of the additional core/water interface created, from ξ_L^2 to $\xi_{L'}^2$, resulting from the core thinning. The contribution of the core chain compression being in fact marginal, the scenario implies $\Delta F_{ci} + \Delta F_\gamma \cong 0$ and thus $fN_2 \ln(\xi_L^2/\xi_{L'}^2) \cong -\gamma\xi_L^2(\xi_{L'}^2/\xi_L^2 - 1)$. Defining the adimensional parameter $\kappa = -\gamma\xi_L^2/fN_2$, the ratio $u = \xi_L^2/\xi_{L'}^2$ of the areas *per* chain in the L and L′ phases is a solution to the nonlinear equation $\ln(u) \cong \kappa(1 - 1/u)$, which can be solved numerically. From contact-angle measurements,[36] we measured a PSAA/water interfacial energy $\gamma = 37.5$ mJ/m^2 and a PSAA/PAA interfacial energy $\gamma = 22.4$ mJ/m^2. From these, taking into account the swelling of the PAA brush, we estimate a PSAA/{water + PAA} interfacial energy of order $\gamma = 35.4$ mJ/m^2 or 8.6 in units of k_BT/nm^2. Given $\xi_L^2 = 2.83$ nm^2 and $N_2 = 133$ and taking $f = 0.33$ (i.e., ionization of the first L′ phase identified, cf. Figure 2b), the solution to the nonlinear equation is $u = 0.335$, from which we compute $\xi_{L'}^2 = 8.45$ nm^2 and $e_{L'} = 1.9$ nm. As ionization is further increased, up to $f = 0.40$ (i.e., ionization of the last L′ phase identified), the solution found is $u = 0.245$, implying $\xi_{L'}^2 = 11.55$ nm^2 and $e_{L'} = 1.4$ nm. These predicted values compare remarkably well to those $e_{L'} = 1.8$ and 1.3 nm (± 0.1 nm), estimated from form factor fitting, which strongly supports the model.

As ionization is increased, the counterion cloud imposes a larger and larger pressure and results in a thinning of the core, as the computation shows. In the meantime, the area per chain increases significantly, yet not enough for the brush to become nonosmotic. Moreover, this increase in the area per chain explains why the dispersions go from milky dispersions to monophasic clear ones at the L to L′ transition: as the area per chain goes from $\xi_L^2 \equiv N_1 a^3/e_L = 2.83$ nm^2 in the frozen-in L phases to $\xi_{L'}^2 \approx N_1 a^3/e_{L'} = \xi_L^2(e_L/e_{L'}) = 8-12$ nm^2 in the molten L′ phases, the amount of water taken in by the polyelectrolyte brush is multiplied by a factor of order up to 4, thereby "sucking in" all the water that was in excess in the last L phase dispersion. As a conclusion, the free energy $F_{L'} = F_{\text{brush}} + F_{\text{core}}$ describes well the physics of these equilibrium swollen lamellar phases as well as the physics of the L to L′ transition resulting from a balance between counterion and interface energetics.

Let us point out here a peculiar experimental fact: we observe that addition of salt results in an increase of the core half-thickness e. For the L′ phases identified at $c_S = 3.4 \times 10^{-1}$, 2.74, and 6.15 M and constant ionization 0.46 (cf. Figure 8c), the fitting of the lamellar form factor gives core half-thicknesses increasing from 1.6 to 1.9 and 2.1 ± 0.05 nm, respectively. Salt seems again to have an effect opposite to that of ionization. To understand this, we can detail the L′ phase thermodynamics as a large amount of salt is added. Given $F_{ci,salt} \approx fN_2[1 + \ln(c_S) + fN_2/2h\xi^2 c_S]$ in salty conditions, $fc_2 \ll c_S$, and conservation of matter $N_1 a^3 \cong e\xi_{L'}^2$ still applies, minimizing anew $F_{L'}$ with respect to h and e leads to

$$\left(\frac{\partial F_{L'}}{\partial h}\right)_e \equiv \left(\frac{\partial F_{\text{brush}}}{\partial h}\right)_e \cong \frac{h}{N_2 a^2} - \frac{f^2 N_2^2 e}{h^2 N_1 a^3 c_S} = 0 \qquad (6)$$

$$\left(\frac{\partial F_{L'}}{\partial e}\right)_h \cong \frac{f^2 N_2^2}{N_1 a^3 h c_S} + \frac{e}{N_1 a^2} - \frac{\gamma N_1 a^3}{e^2} = 0 \qquad (7)$$

Once combined, the two equations yield a nonlinear relation to which e (or h) is a solution. However, noting that the elastic contribution arising from the compression of core blocks is marginal compared to the interfacial cost in eq 7, we easily derive the increase of e with added salt

$$e \cong N_1 a f^{4/5} (a^2\gamma/N_2)^{3/5} (a^3 c_S)^{2/5} \qquad (8)$$

which is in qualitative agreement with our experimental results.

According to eq 8, a scaling law $e \propto c_S^{2/5}$ should be observed, provided the condition $fc_2 \ll c_S$ is satisfied. However, at ionization 0.46, the samples at $c_S = 3.4 \times 10^{-1}$ and 2.74 M

hardly satisfy the condition, as we estimate $fc_2 \approx fN_2e/hN_1a^3$ of the order 0.35 M. These samples are in fact located in the crossover region between salt-free and salty regimes, where the scaling prediction of eq 8 does not exactly apply. More data is needed, in particular in the presence of salt, to verify or refine the thermodynamics of the L′ phase, which we leave to a future paper.

Large Ionization: Details on the S Phase and S′ Phase. There is necessarily a limit to the thinning of the lamellar core in the L′ phase and to the amount of core/water interface that can be created: as the thinning increases with ionization, so do the interfacial cost between core and water and the compression of the core chains, which cannot be neglected anymore. We foresee that the second structural transition, from flat (lamellar) to curved interfaces, corresponds to the limit the counterion cloud can impose on the increase of core/brush interface and core chains compression.

A careful analysis of the SANS data provides a crucial insight. However, the fitting of the form factor features of the SANS spectra must take into account the possibility of penetration of water inside the core, even if the ionization of ($S_{53}A_{39}$) is still not large at $\alpha_{B/A} = 0.46$ (i.e., in the vicinity of pH 7) according to the titration of this block (cf. Figure 6). The scenario of water penetration inside the core is supported by recent results on diblock ($S_{11}A_{12}$)-*b*-A_{229}, equivalent to ($S_{53}A_{39}$)-*b*-A_{133} as far as the composition styrene vs acrylic acid in the first block is concerned but asymmetric in terms of blocks lengths. In the vicinity of pH 7, these diblocks form spherical core−shell objects comprising a water-swollen ($S_{11}A_{12}$) core surrounded by a poly(acrylic acid) brush when concentrated enough.[32] Here, a fully quantitative method is at hand to verify the presence of water inside the core of the S phases identified. The intensity $I(q)$ scattered by a dilute assembly of $N_m = N_p/g$ spherical core−shell objects (where N_p is the number of polymer chains and g is their aggregation number) is simply proportional to the form factor $P_{mic}(q)$ of a single one, i.e., $I(q) \propto N_m P_{mic}(q)$, where[37,38]

$$P_{mic}(q) = g^2\alpha_1^2 F_{core}(q) + g\alpha_2^2 F_{rod}(q) \qquad (9)$$

where $\alpha_1 = \alpha_1' - \alpha_{D_2O}v_1/v_{D_2O}$ and $\alpha_2 = \alpha_2' - \alpha_{D_2O}v_2/v_{D_2O}$ are the excess scattering lengths of the core and the brush chains, respectively, referred to with subscripts 1 and 2, respectively, (α_1', α_2', and α_{D_2O}, respectively, being the scattering lengths of the core, brush, and solvent scatterers, while v_1, v_2, and v_{D_2O} are the corresponding partial molecular volumes). The latter equation is the sum of self-correlation contributions arising from the core and the brush (as well as cross-correlation terms, omitted here as negligible); $F_{core}(q) = 9[\sin(qR_c) - qR_c\cos(qR_c)]^2/q^6R_c^6$ is the normalized form factor of a sphere of radius R_c, while $F_{rod}(q) = 2Si(qh)/qh - [\sin(qh/2)/(qh/2)]^2$ is the form factor of a rodlike PAA chain of length h, where $Si(x) = \int_0^x dt \sin t/t$ is the sine integral function.[39] As was done in previous papers,[3] authorizing water inside the core consists in replacing the aggregation number g with $g(1 - \varphi)$, where φ is the fraction of water inside the core, and recomputing the excess scattering lengths accordingly. This formula was fitted to the experimental SANS spectra, for S phases identified in salt-free conditions for large ionizations (see Figure 2c), as well as in salty ones (see Figure 8c).[40] Nice adjustments to the experimental curves are found. Note that if the aggregation number g were computed from the core volume $g = V_{core}/N_1v_1$, assuming the latter consists only in polymer and is free of water, and the excess scattering lengths densities are taken as those of the blocks, assuming no water inside the core, it is easy to show that the contribution $g\alpha_2^2F_{rod}(q)$ of the stretched A_{133} chains of the brush is largely dominated by that $g^2\alpha_1^2F_{core}(q)$ of a collapsed ($S_{53}A_{39}$) core. Contrary to PS-*b*-PAA systems, which comprise collapsed water-free cores from which most of the scattered intensity originates in the accessible q window, the contribution of a swollen core to the signal decreases as the fraction of heavy water inside the core increases, while the contribution from the stretched chains of the brush becomes visible in the lower q range.

In the intermediate ionization regime (S phase), for the salt-free specimen {$\alpha_{B/A} = 0.46$, $c_S = 0$}, as well as the two salty ones {$\alpha_{B/A} = 0.46$, $c_S = 3.4 \times 10^{-3}$ M} and {$\alpha_{B/A} = 0.46$, $c_S = 3.4 \times 10^{-2}$ M}, the core is found in all cases with a radius of order $R_c = 2.5$nm and an aggregation number of the order 5−6. The inset of Figure 7c shows the superimposition, in absolute scales, of all three curves, which demonstrates that salt has no effect whatsoever on the spherical core radius. Most importantly, no water is needed for the fitting procedure: φ is found equal to 0 in all cases, and we conclude that the cores in these S phases are still essentially water-free, as was also suggested in the previous L′ phases. Finally, while the last L′ phase was found to comprise a water-free lamellar core of half thickness $e_{L'} = 1.3$ nm, the first S phase comprises a water-free spherical core of larger radius $R_c = 2.5$ nm, yet smaller than the size $aN_1^{1/2} \approx 5.4$ nm that core blocks would have in the Gaussian state. Going from L′ to S therefore corresponds to a relaxation of the compression of the core chains.

For the largest ionization investigated (i.e., specimen {$\alpha_{B/A} = 0.64$, $c_S = 0$}, S′ phase), full solubility of the diblock is still not an option since the P(S-*stat*-AA) block is not soluble by itself at this pH. The SANS spectrum shown in Figure 2c cannot be fitted unless a significant amount of water is allowed inside the core: the nicest fit to the experimental data is obtained for $R_c = 3.3$nm and $\varphi = 0.85$ (i.e., 85% of water inside the core), implying a rather small aggregation number (of the order 2−3). However, we recall that water dispersions of diblock ($S_{11}A_{12}$)-*b*-A_{229} were also found to present spherical micelles with small aggregation numbers, above an apparent cmc of order 2−5 wt % at pH 7.[32] In the present case, we foresee that at concentration 5 wt % in water, an ionization $\alpha_{B/A} = 0.64$, and a salt concentration $c_S = 0$, diblock ($S_{53}A_{39}$)-*b*-A_{133} is just above a similar apparent cmc. The ($S_{53}A_{39}$)-*b*-A_{133} structures then seem to shift to minute and highly swollen objects, close to the onset of a self-association. This last result seems like a promising route to follow, when looking for truly self-associating diblocks. The study of this micellization process taking place only for $\alpha_{B/A} \geq 0.64$, as well as the structures obtained at higher concentrations, will be the object of a future paper.

5. Conclusions

We have presented the detailed pH- and salt-dependent lyotropic behavior of a symmetrical amphiphilic P(S-*stat*-AA)-*b*-PAA diblock copolymer, whose specificity is to comprise two weak, like-charged polyelectrolyte blocks with different ionization characteristics. We have demonstrated that this diblock displays several phases depending on the ionization of each block. When the pH of the solution remains smaller than the natural pH in water of the more hydrophobic P(S-*stat*-AA) block, only does the PAA block get ionized, while the P(S-*stat*-AA) block remains water-free and glassy at room temperature. The lamellar phase simply swells with water and displays a long-range smectic order reminiscent of the initial melt state used for the dispersion. The lamellar objects comprise a frozen-in, collapsed P(S-*stat*-AA) core and a swollen PAA brush, in

which counterions are confined in order to satisfy local electroneutrality. The PAA brush then presents all the features of a flat polyelectrolyte brush of constant surface density, i.e., a brush thickness increasing with ionization and decreasing as the ionic strength is increased according to the well-known $c_S^{-1/3}$ scaling. Upon a further increase in pH, the P(S-*stat*-AA) block starts ionizing and the lamellar phase melts. It first undergoes a transition to a second lamellar phase, whose thinner P(S-*stat*-AA) core remains mostly water-free, yet adapts its thickness to external pH and salt conditions. The drive for the transition originates from the pressure imposed by the confined counterion cloud, which induces a decrease in the brush density. The transition can be quantitatively described by the balance between the gain in entropy of mixing of the confined counterions and the enthalpic cost of increasing the amount of interface between the P(S-*stat*-AA) core (still mostly hydrophobic) and the surrounding PAA brush swollen with water. The polyelectrolyte brush itself therefore contributes to the interfacial cost involved in the morphological transitions of strongly amphiphilic diblock copolymers bearing a polyionic moiety. Such participation is consistent with the recent modeling by Grason and Santangelo,[41] of the crucial role of a polyelectrolyte brush in the existence of unexpected transitory structures in dispersed amphiphilic diblock copolymers, like undulated cylinders, usually found in the melt state. The second lamellar phase identified here, with a thinning core, could very well be another example of the same principle.

It appears that curvature, which one would usually expect as the brush becomes more charged, does not occur first. It is apparently more profitable for the system to make the core thinner than to curve it. As a matter of fact, curvature eventually appears when ionization is further increased, since core−coronal objects of spherical symmetry are finally found. The core, however, remains again mostly water-free according to our small-angle data fitting. The present study therefore provides an overview of the complex structural behavior that a single P(S-*stat*-AA)-*b*-PAA diblock copolymer can offer. In particular, we have presented detailed experimental evidence of two original properties. The occurrence of a transition from a frozen-in to a molten system controlled by the pH, and most importantly, morphological transitions triggered by the pH and the ionic strength of the solutions, are both potential first steps toward water-based responsive materials.

Acknowledgment. The authors are thankful to Mathieu Joanicot (Rhodia's Laboratory of the Future, Pessac, France) for guidance, Gilda Lizarraga (Rhodia's Research and Technological Center, Bristol, USA) for help in the synthesis, Charlotte Basire (Rhodia's Research and Technological Center, Lyon, France) for providing the AFM picture, and Loïc Auvray and the Laboratoire Léon Brillouin (Commissariat à l'Energie Atomique and CNRS, Saclay, France) for access to the small-angle neutron scattering facilities.

Appendix A

The dispersion of A_{111} in the absence of NaOH ($\alpha_{B/A}^{(2)} = 0$) is slightly turbid, of starting $pH_{0,0}^{(2)} = 2.5$. It becomes totally transparent as soon as $\alpha_{B/A}^{(2)} \geq 0.018$ ($pH^{(2)} \geq 2.80$), that is, for a very low addition of NaOH. This curve in fact presents the classical features of the titration of a neat polyelectrolyte, as we briefly explain in the following. The chemically dissociated fraction α of an acid AH is: $\alpha = [A^-]/([A^-] + [AH])$, where AH and A^- are the neutral and ionic forms of the acid, respectively. This quantity is generally computed knowing the value of the constant of dissociation K_A, defined as: $K_A = [A^-][H^+]/[AH]$. Combining the two previous equations, $pK_A \equiv -\log K_A$ and $pH \equiv -\log [H+]$ are linked through the well-known Henderson−Hasselbach equation: $pK_A \equiv pH + \log((1 - \alpha)/\alpha)$. Thus, α can be computed for any given pH, provided the pK_A of the polymeric electrolyte is accurately known. For weak acids, the Henderson−Hasselbach equation often turns out to be linear in α:[42] the inflection point $\partial^2\alpha/\partial pK_A^2 = 0$ then exactly coincides with that of $\partial^2\alpha/\partial pH^2 = 0$ at half titration. At this point, the pH is simply equal to the pK_A of the acid.

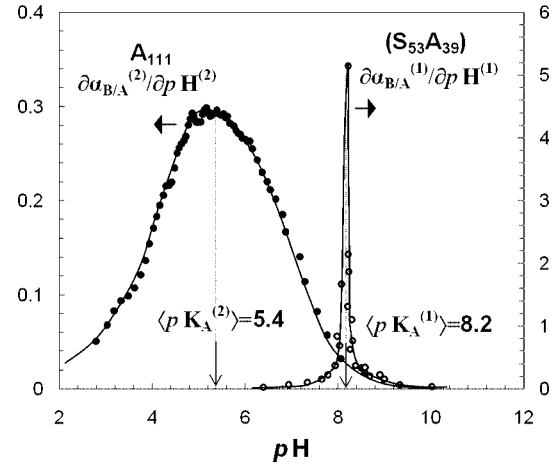

Figure 13. Derivatives $\partial\alpha_{B/A}^{(1)}/\partial pH^{(1)}$ and $\partial\alpha_{B/A}^{(2)}/\partial pH^{(2)}$ of the titration curves of Figure 5 of, respectively, $(S_{53}A_{39})$ and A_{111} both at 2.5 wt % in salt-free water. The lines are guide for the eye.

In Figure 13, we plot the derivative $\partial\alpha_{B/A}{}^{(2)}/\partial pH^{(2)}$ of the titration curve of A_{111} at 2.5 wt % in salt-free water shown in Figure 5. The derivative shows a well-defined but very broad bump over the entire pH range. The locus of its maximum, which corresponds to an inflection point reached at half-titration, i.e., $\partial^2\alpha_{B/A}^{(2)}/\partial pH^2 = 0$ for $\alpha_{B/A}^{(2)} = 1/2$, is identified with the mean apparent $\langle pK_A\rangle$ of the polyacid A_{111} at 2.5 wt % in salt-free water: $\langle pK_A{}^{(2)}\rangle = 5.4$, larger than that $pK_A = 4.5$ of the acrylic acid monomer. Indeed, while the pK_A value is unique and well-defined for a monomeric acid, weak polyelectrolytes such as poly(acrylic acid), usually display an apparent broad pK_A distribution with a mean apparent $\langle pK_A\rangle$ value larger than that of its monomeric constituent. The phenomenon is due to the polymer architecture and originates from the interactions between neighbor sites along the polymer chain: the presence of an already ionized site diminishes the ionizability of the neighbors,[43] resulting in an apparent larger pK_A.[44,45]

On the other hand, the dispersion of $(S_{53}A_{39})$ in the absence of NaOH (i.e., $\alpha_{B/A}^{(1)} = 0$) is a stable, milky dispersion, of starting pH: $pH_{0,0}^{(1)} = 4.9$. The dispersion remains milky as titration proceeds up to $\alpha_{B/A}^{(1)} = 0.75$ (i.e., $pH^{(1)} = 8.4$), beyond which it becomes turbid. While A_{111} is a pure polyelectrolyte, fully soluble in water as soon as a few charges have been created, $(S_{53}A_{39})$ requires a much larger amount of NaOH (i.e., a much larger pH) to become soluble in water $\alpha_{B/A}^{(1)} \geq 0.75$ (i.e., pH $\geq$ 8.4). The titration curves shown in Figure 6 in fact present two major differences: (i) the titration curve of $(S_{53}A_{39})$ is entirely shifted to larger pH values, compared to that of A_{111}; (ii) the titration of $(S_{53}A_{39})$ shows a broad plateau, in contrast with that of A_{111} (the pH of the latter steadily increases with ionization over the entire titration range). Note that the plateau observed in the titration of $(S_{53}A_{39})$ shown in Figure 5 results in the derivative $\partial\alpha_{B/A}^{(1)}/\partial pH^{(1)}$ of Figure 13 in a well-defined, very narrow peak centered on $pH_{plateau}^{(1)} = 8.2$. Both the presence of the plateau and the vertical shift, generally not observed in the titration curve of a pure polyelectrolyte, have already been

reported for the titration of a poly((methacrylic acid)-*stat*-(ethylacrylate)) statistical copolymer ($EA_{6150}MAA_{3850}$), with approximately $^1/_3$ of methacrylic acid units.[46] The authors then discussed the nature and origin of these peculiar features by means of self-consistent mean-field computations, and demonstrated that both the plateau and the vertical shift can be attributed to electrostatic correlations between the dissociation of neighbor ionizable sites along the chain.

Appendix B

The theoretical expression for the structure factor $S(q)$ of a smectic array of lamellar objects has been thoroughly addressed, in particular for surfactant systems. To describe the scattering patterns obtained for such systems with small-angle techniques, different models have been developed, of which one may count:[47] (i) the paracristal (PC) models relying on positional disorder of the first or second kind in the smectic order; (ii) the modified Caillé theory (MCT) relying on fluctuations in the very shape of the membrane. Both models (i.e., either positional disorder or membrane fluctuations) aim at describing the decrease in the successive structure factor peaks intensities usually observed in surfactant lamellar phases. On the other hand, experimental literature is scarce for polymeric L phases. None of the spectra obtained with our polymeric L phases can be fitted by models taking into account fluctuations in the smectic order or in the membrane shape, which suggests that such phenomena are not at work here. In fact, positional fluctuations, if permitted, would necessarily result in a compression of brushes and therefore in a high energy penalty due to the osmotic pressure of the Na^+ counterions confined within the brush. The osmotic nature of PAA brushes induces a very high compression modulus for the L phase, and we believe that the existence of positional fluctuations is impossible. On the other hand, fluctuations in the membrane shape are not possible either, as long as the core of the membrane remains glassy: considering ($S_{53}A_{39}$) is glassy at room temperature as long as it remains dehydrated, the L phase is most certainly unable to fluctuate, the bending modulus of its glassy ($S_{53}A_{39}$) core being too large. Finally, the disorder in the lamellar phase only originates from defects and mosaicity. Provided the multiplicity of any reflection of order k, $k \geq 1$, is equal to 1 in an L phase, our modeling assumes the decrease of the successive peak intensities to be solely due to the form factor envelop. Considering a negligible polydispersity of the domain thicknesses, the ratio of the kth order peak intensity measured $S_k = (kq^*)^2 I(kq^*)$ positioned at $q = kq^*$, $k \geq 1$, over that $S_1 = q^{*2} I(q^*)$, of the first order positioned at $q = q^*$, is a function of the form factor $P_L(q)$ only

$$\frac{S_k}{S_l} \equiv \frac{(kq^*)^2 I(kq^*)}{q^{*^2} I(q^*)} = \frac{\sin^2(k\pi\Phi)}{k^2 \sin^2(\pi\Phi)} \qquad (10)$$

By definition, the quantity $\Phi = 2e/d$ varies from 0 to 1: it is simply the volume fraction of the lamellar sublayer of thickness $2e$ in the total spacing d, while $1 - \Phi = 2h/d$ is the volume fraction of the other sublayer. As such nonlinear equation is symmetrical with respect to $\Phi = {}^1/_2$ regardless of the value of k, $(1 - \Phi)$ is necessarily an eigenvalue if Φ is. Consequently, the corresponding values computed for e and h are readily exchangeable from a mathematical point of view. However, only one couple of values makes sense from a physical point of view: because of the difference in solubility of the two constitutive blocks ($S_{53}A_{39}$ and A_{133}, it is reasonable to choose the eigenvalues so that the smaller one e corresponds to the ($S_{53}A_{39}$)-rich sublayer, while the larger one h corresponds to the A_{133}-rich sublayer. Note that, for $0 \leq \Phi \leq 1$, the values taken by the nonlinear function expressed in above equation verify: $0 \leq S_k/S_1 \leq 1$, regardless of the value of k, which physically makes sense, since in the small-angle spectrum of a L phase, the kth order peaks, $k > 1$, usually have intensities smaller than the first order $k = 1$. For $k \geq 3$, the nonlinear equation possesses from 2 to $2(k - 1)$ eigenvalues, but only 2 for $k = 2$, which are the only 2 common eigenvalues of all equations of order k, $k \geq 2$: these are the two symmetric eigenvalues that have to be solved for. Measuring the intensities of several successive peaks on the $q^2I(q)$ vs q plots, and solving numerically the above nonlinear equation for the only unknown parameter Φ, allows for the direct computation of $e = \Phi d/2$ and $h = d/2 - e = (1 - \Phi)d/2$.

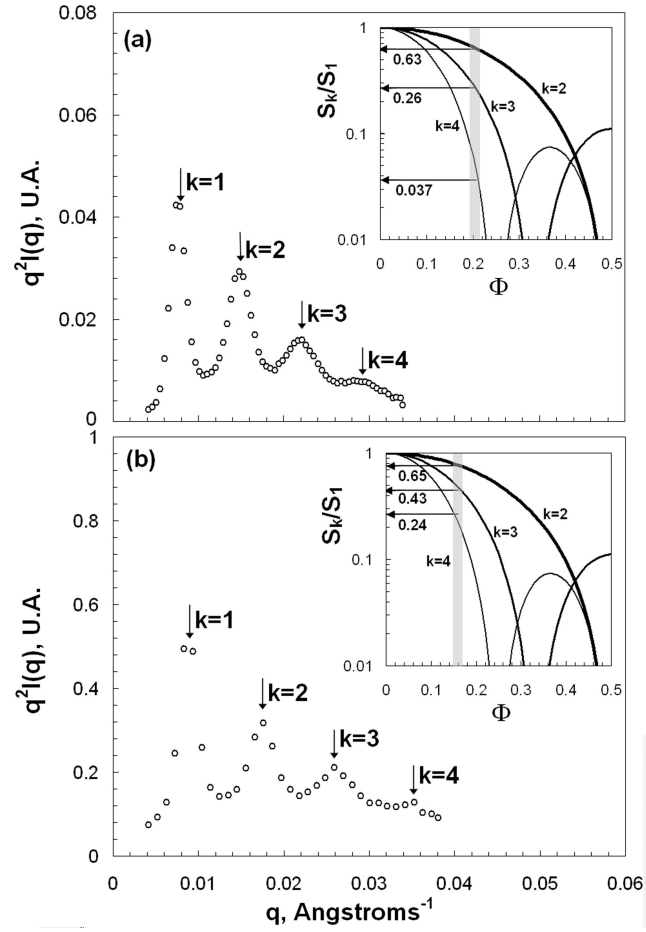

Figure 14. Typical SANS spectra of: (a) diblock S_{83}-*b*-A_{123} in water, obtained at diblock concentration 5 wt % for $\alpha_{B/A} = 0.30$ and $c_S = 0$; (b) diblock ($S_{53}A_{39}$)-*b*-A_{133} in water, at diblock concentration 5 wt % for $\alpha_{B/A} = 0.27$ and $c_S = 0$, both showing several structure peaks. Inserts: calculated functions S_k/S_1 as a function of object volume fraction Φ, for $k = 2$, 3, and 4.

This computational procedure is tested on a spectrum of the reference diblock S_{83}-*b*-A_{123}, obtained on a frozen swollen L phase formed in water at $\alpha_{B/A} = 0.30$. In Figure 14a, we plot the SANS spectra $q^2I(q)$ vs q, from which we extract the ratios of the intensities of the second, third, and fourth correlation peaks over that of the first peak: $S_2/S_1 = 0.63$, $S_3/S_1 = 0.26$, and $S_4/S_1 = 0.037$. In the insert of Figure 14b, we plot the three theoretical functions calculated according to the previous equation for $k = 2$, 3, and 4. Within a reasonable margin of error, the intercepts between the different theoretical functions and the corresponding experimental values lead to the same value for Φ, i.e., $\Phi = 0.187 \pm 0.010$. Given the position $q^* = 0.0073$ Å^{-1} of the first correlation peak, we compute the lamellar

period to be $d = 85.7$ nm, from which the half thickness $e = \Phi d/2 = 8.0 \pm 0.4$ nm of the S_{83} sublayer is computed, consistent with the value 8.1 ± 0.1 nm measured in the initial melt state. Therefore, we consider our computational method accurate and apply it to the L phases formed by the $(S_{53}A_{39})$-*b*-A_{133} in water. An example is shown in Figure 14b.

References and Notes

(1) (a) *Dynamics of surfactant self-assemblies: micelles, microemulsions, vesicles, and lyotropic phases*; Raoul Z., Ed.; CRC Press, 2005; Vol. 125. (b) *Adsorption and aggregation of surfactants in solution*; Mittal, K. L. , Shah, D. O., Eds.; Marcel Dekker, 2003; Vol. 109

(2) *Polymeric surfactants*; Piirma, I., Ed.; Marcel Dekker: 1992.

(3) Goldmints, I.; Holzwarth, J. F.; Smith, K. A.; Hatton, T. A. *Langmuir* **1997**, *13*, 6130.

(4) (a) Creutz, S.; van Stam, J.; De Schryver, F. C.; Jérôme, R. *Macromolecules* **1998**, *31*, 681. (b) Jada, A.; Siffert, B.; Riess, G. *Colloids Surf. A* **1993**, *75*, 203. (c) Antoun, S.; Gohy, J.-F.; Jérôme, R. *Polymer* **2001**, *42*, 3641. (d) Chang, Y.; Bender, J. D.; Phelps, M. V. B.; Allcock, H. R. *Biomacromolecules* **2002**, *3*, 1364.

(5) Rager, T.; Meyer, W. H.; Wegner, G. *Macromolecules* **1997**, *30*, 4911.

(6) Bendejacq, D.; Joanicot, M.; Ponsinet, V. *Eur. Phys. J. E* **2005**, *17*, 83.

(7) (a) Burguière, C.; Pascual, S.; Bui, C.; Vairon, J.-P.; Charleux, B.; Davis, K. A.; Matyjaszewski, K.; Betremieux, I. *Macromolecules* **2001**, *34*, 4439. (b) Save, M.; Manguian, M.; Chassenieux, C.; Charleux, B. *Macromolecules* **2005**, *38*, 280.

(8) Romet-Lemonne, G.; Daillant, J.; Guenoun, P.; Holley, D.; Mays, J. W. *J. Chem. Phys.* **2005**, *122*, 064703.

(9) Bhatia, S. R.; Mourchid, A.; Joanicot, M. *Curr. Opin. Colloid Interface Sci.* **2001**, *6*, 471.

(10) (a) Yamanioto, Y.; Yasugi, K.; Harada, A.; Nagasaki, Y.; Kataoka, K. *Journal of controlled release* **2002**, *82*, 359. (b) Riley, T.; Stolnik, S.; Heald, C. R.; Xiong, C. D.; Garnett, M. C.; Illum, L.; Davis, S. S.; Purkiss, S. C.; Barlow, R. J.; Gellert, P. R. *Langmuir* **2001**, *17*, 3168. (c) Lavasanifar, A.; Samuel, J.; Kwon, G. S. *Adv. Drug Deliv. Rev.* **2002**, *54*, 169.

(11) *"Solubilization in Surfactant Aggregates*; Sherril D. C., Scamehorn J. F. , Eds.; Marcel Dekker: 1995; Vol. 55.

(12) Corpart, P.; Charmot, D.; Zard, S. Z.; Biadatti, T.; Michelet, D. US Patent 6,153,705, Nov 28, 2000.

(13) Destarac, M.; Charmot, D.; Franck, X.; Zard, S. Z. *Macromol. Rapid Commun.* **2000**, *21*, 1035.

(14) Charmot, D.; Corpart, P.; Adam, H.; Zard, S. Z.; Biadatti, T.; Bouhadir, G. *Macromol. Symp.* **2000**, *150*, 23.

(15) Borisov, O. V.; Zhulina, E. B. *Langmuir* **2005**, *21*, 3229.

(16) (a) Tran, Y.; Auroy, P.; Lee, L. T. *Macromolecules* **1999**, *32*, 8952. (b) Guenoun, P.; Schalchli, A.; Sentenac, D.; Mays, J. W.; Benattar, J. J. *Phys. Rev. Lett.* **1995**, *74*, 3628. (c) Balastre, M.; Li, F.; Schorr, P.; Yang, J.; Mays, J. W.; Tirrell, M. *Macromolecules* **2002**, *35*, 9480. (d) Ahrens, H.; Förster, S.; Helm, C. A. *Phys. Rev. Lett.* **1998**, *81*, 4172.

(17) (a) Pincus, P.; Witten, T. *Europhys. Lett.* **1987**, *3*, 315. (b) Pincus, P. *Macromolecules* **1991**, *24*, 2912. (c) Ross, R. S.; Pincus, P. *Macromolecules* **1992**, *35*, 2177.

(18) (a) Borisov, O. V.; Zhulina, E. B.; Birshtein, T. M. *Macromolecules* **1994**, *27*, 4795. (b) Borisov, O. V.; Birshtein, T. M.; Zhulina, E. B. *J. Phys. II France* **1991**, *1*, 521.

(19) Csajka, F. S.; Netz, R. R.; Seidel, C.; Joanny, J.-F. *Eur. Phys. J. E* **2001**, *4*, 505.

(20) Groenewegen, W.; Lapp, A.; Egelhaaf, S. U.; van der Maarel, J. R. C. *Macromolecules* **2000**, *3283* (33), 4080.

(21) Forster, S.; Abetz, V.; Muller, A. H. E. *Adv. Polym. Sci.* **2004**, *166*, 173.

(22) Shen, H.; Zhang, L.; Eisenberg, A. *J. Am. Chem. Soc.* **1999**, *121*, 2728.

(23) Zhang, L.; Eisenberg, A. *Macromolecules* **1996**, *29*, 8805.

(24) Geng, Y.; Ahmed, F.; Bhasin, N.; Discher, D. E. *J. Phys. Chem. B* **2005**, *109*, 3772.

(25) Bendejacq, D.; Ponsinet, V.; Joanicot, M.; Loo, Y.-L.; Register, R. A. *Macromolecules* **2002**, *35*, 6645.

(26) Bendejacq, D.; Ponsinet, V.; Joanicot, M.; Vacher, A.; Airiau, M. *Macromolecules* **2003**, *36*, 7289.

(27) Bendejacq, D.; Ponsinet, V. *Eur. Phys. J. E* **2004**, *13*, 3.

(28) In spite of approximately equal molecular weights (i.e., 16 kg/mol), $(S_{53}A_{39})$-*b*-A_{133} and S_{83}-*b*-A_{123} produce L phases of different characteristic sizes in the melt state, as a direct consequence of the effective Flory−Huggins interaction parameter χ_{eff} between the two constitutive blocks: because of its statistical copolymerization with a significant amount of AA motives, $(S_{53}A_{39})$ has an incompatibility with A_{133} smaller than that of S_{83} with A_{123}. The most remarkable repercussion of this feature is that $(S_{53}A_{39})$-*b*-A_{133} forms a bilayer thinner and less dense in terms of surface chain density than that of S_{83}-*b*-A_{123}.

(29) Guinier, A.; Fournet, G. *Small-Angle Scattering of X-Rays*; Wiley & Sons: New York, 1955.

(30) Porod, G. *Small-Angle X-ray Scattering*; Glatter, O. , Kratky, O. , Eds.; Academic Press: London, 1982.

(31) This formula is valid provided the scattering lamellar object can be considered as infinite, i.e., their thickness of the lamellae is much smaller than its lateral dimension.

(32) Bendejacq, D.; Ponsinet, V.; Joanicot, M. *Langmuir* **2005**, *21*, 1712.

(33) The derivative $\partial\alpha_{B/A}/\partial$pH *vs* pH, however, still clearly shows two distinct contributions to ionization, one broad in the small pH range and the other much narrower in the large pH range. These, as before, are associated with the distinct ionizations of the two constituting blocks. However, the average apparent $pH_{plateau}$ and $\langle pK_A \rangle$ of the blocks in the diblock, 7.43 and 6.07 for $(S_{53}A_{39})$ and A_{111}, respectively, are slightly different from those measured when the blocks were titrated as a mixture, i.e., 7.90 and 5.75. Therefore, the topological link in diblock $(S_{53}A_{39})$-*b*-A_{133}, seems to have a slight additional effect on the respective ionizations of the two blocks. As far as the purely acrylic acid block A_{133} is concerned, this increase in the apparent $\langle pK_A \rangle$ may be attributed to a hindered polyelectrolyte structure resulting from the self-association in water, by analogy with what was observed with a poly(acrylic acid) covalently attached to a polyamide matrix (cf. ref 34) therefore restricted in terms of conformational entropy.

(34) Healy, E. M.; Ramsley, A. O.; Natsios, B. A. *J. Appl. Polym. Sci.* **2003**, *16*, 37.

(35) Note also that the pH of the L′ phase crosses $pH_{c1} = 4.9$ when $c_s = 1.6$ M, which may be the locus of a L ′ to L transition.

(36) Bendejacq, D.; Ponsinet, V. To be submitted as a note to the editor of *Macromolecules*.

(37) (a) Pedersen, J. S.; Gerstenberg, M. C. *Macromolecules* **1996**, *29*, 1363. (b) Pedersen, J. S. *J. Chem. Phys.* **2001**, *114*, 2839.

(38) Muller, F.; Delsanti, M.; Auvray, L.; Yang, J.; Chen, Y. J.; Mays, J. W.; Demé, B.; Tirrell, M.; Guenoun, P. *Eur. Phys. J. E* **2000**, *3*, 45.

(39) Higgins, J. S.; Benoit, H. C. *Polymers and Neutron Scattering*; Clarendon Press: Oxford, 1994.

(40) The fitting procedure minimizes the reduced χ^2 parameter $\chi_r^2 = 1/(n-p)\Sigma[q_i^2 I^{exp}(q_i) - q_i^2 I^{comp}(q_i)]^2/\sigma^2(q_i)$, where n is the number of experimental points, p that of adjustable parameters, $I^{exp}(q_i)$ and $I^{comp}(q_i)$, the experimental and computed intensities at wave-vector q_i, respectively, and $\sigma(q_i)$, the experimental standard deviation at wave-vector q_i.

(41) Grason, G. M.; Santangelo, C. D. *Eur. Phys. J. E.* **2005**, *20*, 335.

(42) Borkovec, M.; Jönsson, B.; Koper, G. J. M. Ionization Processes and Proton Binding in Polyprotic Systems: Small molecules, Proteins, Interfaces and Polyelectrolytes. In *Surface and Colloid Science*; Matijevic, E., Ed.; Kluwer Academic, Plenum Press: New York, 2001; Vol. 16, pp 19−339.

(43) Annenkov, V. V.; Kruglova, V. A.; Mazyar, N. L. *J. Polym. Sci., Part B: Polym. Phys.* **1998**, *36*, 931.

(44) Borkovec, M.; Daicic, J.; Koper, G. J. M. *Proc. Natl. Acad. Sci. U.S.A.* **1997**, *94*, 3499.

(45) (a) Kitano, T.; Kawaguchi, S.; Ito, K.; Minakata, A. *Macromolecules* **1987**, *20*, 1598. (b) Cleland, R L. *Macromolecules* **1982**, *15*, 386. (c) Ullner, M.; Jönsson, B.; Peterson, C. *J. Chem. Phys.* **1996**, *104*, 3048.

(46) Borukhov, I.; Andelman, D.; Borrega, R.; Cloitre, M.; Leibler, L.; Orland, H. *J. Phys. Chem. B* **2000**, *104*, 11027.

(47) Nallet, F.; Laversanne, R.; Roux, D. *J. Phys. II* **1993**, *3*, 487.

JP712015H